Origin of Thermohaline Staircases

WILLIAM J. MERRYFIELD

Institute of Ocean Sciences, Sidney, British Columbia, Canada

ABSTRACT

Hypotheses concerning the origin of thermohaline staircases in salt fingering regions are reviewed and assessed. One such hypothesis, that staircases arise from thermohaline intrusions, is developed into a quantitative theory. It is shown that growing intrusions evolve toward staircases when the background density ratio lies below a threshold value, and nonlinear computations confirm that staircases are viable intrusion equilibria. Staircase properties such as step heights, lateral density ratios, and layer slopes lie closest to observed values when salt fingers are assumed not to contribute to shear stress and when turbulent mixing rates are smaller than usual thermocline values.

1. Introduction

Thermohaline staircases are striking sequences of mixed layers, ranging from tens to hundreds of meters thick, separated by steep-gradient interfaces, which are typically several meters thick. Staircases are found where large-scale temperature T and salinity S both increase upward in a manner that favors vigorous salt fingering (Schmitt 1994).[1]

Well-developed staircases have been observed beneath the Mediterranean outflow (Tait and Howe 1968; Howe and Tait 1970; Zenk 1970; Elliott et al. 1974), in the Western Mediterranean (Johannessen and Lee 1974; Zodiatis and Gasparini 1996; Krahmann 1997) and northeast Caribbean (Lambert and Sturges 1977), and throughout the region of the C-SALT observing program in the western tropical North Atlantic (Mazeika 1974; Boyd and Perkins 1987; Schmitt et al. 1987; Boyd 1989). Less distinct examples have been noted in the Sargasso Sea (Cooper and Stommel 1968) and the eastern equatorial Pacific (Miller and Browning 1974).

Thermohaline staircases are distinguished by their extreme stability in space and time. Individual steps have been traced laterally for upwards of 100 km (Elliott et al. 1974; Johannessen and Lee 1974; Schmitt 1988),

and can persist several years or more (Johannessen and Lee 1974; Molcard and Tait 1977).

The connection between staircases and salt fingering was suggested by Turner (1967) and Stern and Turner (1969), who noted that the vertical gradients in oceanic staircases favor fingering, and also that laboratory experiments can produce analogous structures in which salt fingers occupy the high-gradient interfaces, and drive convection in the adjoining mixed layers. The occurrence of salt fingers in the interfaces of oceanic staircases has been established by microstructure measurements (Magnell 1976; Lueck 1987; Marmorino et al. 1987; Fleury and Lueck 1991) and optical imaging (Williams 1975; Kunze et al. 1987). Observations also provide evidence of convective plumes in the mixed layers (Marmorino et al. 1987).

Several hypotheses have been put forth for how thermohaline staircases might develop from initially uniform gradients of T and S. This paper first reviews three such hypotheses: that staircases arise from an instability of salt fingers (section 2), that they are metastable equilibria induced by external disturbances (section 3), and that they arise because salt fingers effect negative density diffusion (section 4). In section 5, the hypothesis that staircases arise from thermohaline intrusions is developed into a quantitative theory. (Readers interested primarily in a proposed solution to the staircase problem should skip to this section.) From linear theory it is shown that intrusions can evolve toward a staircase configuration featuring alternating fingering and convective layers, provided the density ratio lies below a threshold value. An analytical criterion for this threshold that depends on mixing rates, property gradients, as well as the heights, slopes, and growth rates of the intrusions is derived. Nonlinear calculations confirm that intru-

---

[1] Sequences of steps which are typically an order of magnitude thinner appear where T and S both increase downward, conditions that favor diffusive convection (e.g., Neshyba et al. 1971; Padman and Dillon 1987; Muench et al. 1990.) In this paper, attention is confined primarily to the salt fingering case.

Corresponding author address: Dr. William Merryfield, Institute of Ocean Sciences, Sidney, BC V8W 4B2, Canada.
E-mail: merryfieldw@dfo-mpo.gc.ca

sions can equilibrate as staircases and suggest that the relatively high vertical gradients in staircase interfaces are maintained by shearing of large-scale horizontal gradients. Assuming plausible salt-fingering flux laws, the theory best reproduces observed staircase properties when the turbulent mixing coefficient is small (<0.1 cm^2 s^{-1}), the turbulent Prandtl number is of order unity, and salt fingers do not contribute to viscous stress. A summary and conclusions are presented in section 6.

Before proceeding, a few facts about salt fingers and some terminology are briefly reviewed. (For a comprehensive review, see Schmitt 1994.) Salt fingering occurs when a stably stratified component (temperature T) diffuses more rapidly than an unstably stratified component (salinity S). Fingering is characterized by three dimensionless parameters: molecular Prandtl number $\sigma = \nu/\kappa_T$, where ν is viscosity and κ_T is thermal diffusivity; inverse Lewis number $\tau = \kappa_S/\kappa_T$, where κ_S is the diffusivity of salt; and density ratio $R_\rho = \alpha T_z/\beta S_z$, where T_z is the stabilizing vertical temperature gradient, S_z is the destabilizing vertical salinity gradient, α is the coefficient of thermal expansion, and β is the coefficient of saline contraction. Values $\sigma = 7$ and $\tau = 0.01$ characteristic of seawater are assumed except where noted. Salt fingers are linearly unstable for $1 < R_\rho < \tau^{-1}$, and produce observable effects in the ocean primarily when $R_\rho \lesssim 4$. In the sections that follow, reference is occasionally made to laboratory experiments in which the slower and faster diffusing components are sugar and salt. In such instances, S is identified with sugar and T with salt.

2. Collective instability of salt fingers

In investigating the stability of steady, vertically uniform salt fingers at large Prandtl number, Stern (1969) found that collections of fingers should excite internal gravity waves when a dimensionless parameter (equivalent to a finger Reynolds number) exceeds a critical value of order unity. The instability criterion, as later refined by Holyer (1981), is

$$\frac{\beta F_S - \alpha F_T}{\nu(\alpha T_z - \beta S_z)} > \frac{1}{3}, \qquad (2.1)$$

where F_T and F_S represent vertical fluxes of temperature and salinity. This parameter and its variants have become known as the Stern number.[2]

Stern (1969) speculated that this collective instability of salt fingers might be instrumental in generating stepped structures from initially uniform gradients. In Stern's scenario, growing salt fingers generate internal

waves, which disrupt the fingers in regions of large vertical shear. Convection sets in, driven by buoyancy fluxes from adjoining interfaces in which salt fingers survive. Direct evidence for this scenario comes from qualitative observations of developing fingers. For example, Stern and Turner (1969), describing laboratory experiments in which a mixed layer of sugar solution was placed over a linearly stratified salt solution, reported that "Intermittent sideways oscillations of the fingers are followed by stronger horizontal motions until large-scale vertical convection is established. . . ."

Additional evidence is provided by the fact that many laboratory salt fingering interfaces exhibit Stern numbers of order the critical value (Linden 1973; Schmitt 1979; Taylor and Bucens 1989), although McDougall and Taylor (1984) reported Stern numbers as high as 5 at low R_ρ. Experiments where salt and sugar replace heat and salt as the faster and slower diffusing components have Prandtl number (defined here as the ratio of viscosity to diffusivity of the faster-diffusing solute) $\sigma \approx 700$ and hence should reflect predictions of the collective instability theory at least as well as heat–salt fingers ($\sigma \approx 7$). Stern numbers in salt–sugar fingering interfaces have been found to range from 0.002 (Lambert and Demenkow 1971) to 0.006 (Griffiths and Ruddick 1980).[3] The apparent discrepancy with (2.1) could indicate that the stability of growing and finite-length fingers has some further dependence on σ and τ or that the Stern (1969) scenario does not govern fingering interfaces under these conditions.

An issue connected with the Stern (1969) hypothesis concerns the nature of salt finger instability. Subsequent stability calculations for steady fingers have shown that small-scale zigzag or varicose modes generally grow faster than collectively excited gravity waves (Holyer 1984; Howard and Veronis 1992). Shen (1995) extended the analysis to growing fingers and showed that varicose modes grow faster than oscillatory modes and faster than the fingers themselves. In numerical experiments initialized with large-amplitude growing salt fingers, the varicose instability appears to govern finger breakdown (Whitfield et al. 1989; Shen 1995), although such simulations might not encompass enough fingers for collective instability to be adequately represented.

A further unresolved question concerns the conditions under which the Stern (1969) scenario operates. Stern and Turner (1969) reported that layers formed when a sharp T and S interface was present initially and when a mixed layer of sugar solution was placed over a linearly stratified salt solution as described above. How-

---

[2] The result (2.1) applies to two-dimensional (planar) salt fingers. An extension of the stability analysis to three-dimensional fingers having rectangular planforms yields a critical Stern number of 2/3 (Holyer 1985). Kunze (1987, 1995) considered a similar instability criterion in terms of a finger Richardson or Froude number.

[3] Based on $R_\rho = 1.7$, $\beta F_S = 1.0 \times 10^{-6}$ cm s^{-1}, $\alpha F_T = 0.88\beta F_S$, $\nu = 0.01$ cm^2 s^{-1} and $\beta = 0.68$ for Griffiths and Ruddick (1980) experiment 2, assuming $S_z = \Delta S/h$, with interfacial contrast $\Delta S = 1.4\%$ and thickness $h = 3.5$ cm. For $R_\rho = 1.03$, $\beta F_S = 1.6 \times 10^{-4}$ cm s^{-1}, $\alpha F_T = 0.93\beta F_S$, $\Delta S = 7.8\%$, and $h < 0.1$ cm yields an upper limit for Stern number of 0.007.
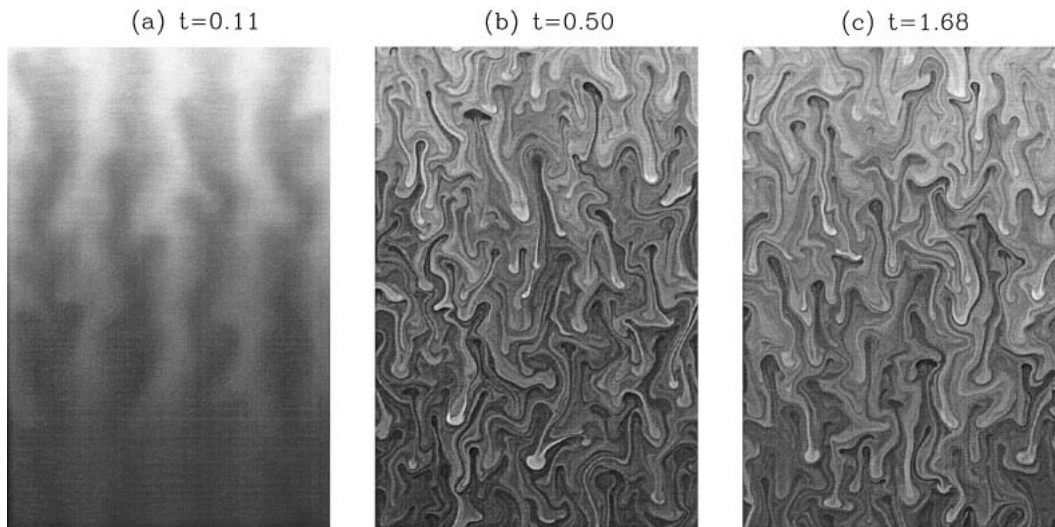
(a) t=0.11   (b) t=0.50   (c) t=1.68

FIG. 1. Evolution of ''salinity'' (slower-diffusing solute) in a numerical experiment having the same parameter values and initial conditions as that of Özgökmen et al. (1998), but with periodic rather than solid upper and lower boundaries. Lighter shades represent higher concentrations, and darker shades lower concentrations. (a) At $t = 0.11$ initial sinusoidal perturbations have grown to become fingers, which in turn are becoming unstable to smaller, faster-growing fingers. (b) The smaller fingers soon dominate, and by $t = 0.50$ a statistically uniform equilibrium has been established. (c) This state persists, and at later times shows no signs of developing convective layers.

ever, when T and S gradients were both initially present, the outcome depended upon the care with which the initial stratification was established. Disturbances imposed deliberately during the filling process grew and triggered convection, whereas experiments that were set up carefully exhibited vertically uniform fingering. The latter outcome is typical of numerical experiments having initially uniform T and S gradients (Whitfield et al. 1989; Shen 1995; Merryfield and Grinder 2000, manuscript submitted to *J. Phys. Oceanogr.,* hereafter MG).

An exception is the simulation of Özgökmen et al. (1998) in which the upper and lower boundaries are solid and insulating, rather than periodic as in other investigations. They chose system parameters so that the combined layer and interface thicknesses as predicted by Stern (1969) would fit within the computational domain. Additional requirements that fingers be adequately resolved and that interface thickness be an appreciable fraction of the layer thickness led them to adopt $\sigma = 100$ and $\tau = 1/30$. In this simulation a well-defined fingering interface develops, with convective layers above and below. However (as the authors acknowledge), this appears most likely to be due to convergence of buoyancy flux at the solid boundaries.

To examine the possibility that collective instability plays a role in forming the Özgökmen et al. (1998) layer–interface structure, a similar calculation was undertaken in which the solid upper and lower boundaries were replaced by periodic boundary conditions. Details of the pseudospectral numerical algorithm are described in MG. Figure 1 depicts salinity over the range of times recorded in the Özgökmen et al. Figs. 4, 5, and 6. As in Özgökmen et al., a large sinusoidal perturbation was

imposed on the the initial salinity field. This perturbation has a longer horizontal wavelength than the fastest-growing salt fingers. At time $t = 0.11$ (Fig. 1a), the initial perturbation has developed into fingers, which have become ''feathered'' due to smaller-scale perturbations growing more rapidly. This phenomenon resembles the instability of wide fingers in a Hele Shaw cell subject to a sudden increase in gravity (cf. Fig. 2 of Taylor and Veronis 1996) and is evident in Fig. 4 of Özgökmen et al. At later times the most unstable scales dominate, and a statistical equilibrium is established in which fingering and mean solute gradients remain nearly uniform (Figs. 1b,c). Because fluxes of solute leaving the bottom of the domain are continually replenished at the top, the system does not subsequently ''run down'' as in Özgökmen et al.

The absence of layer formation in this calculation suggests that layer formation from initially uniform gradients as observed by Özgökmen et al. (1998) is strongly influenced by their choice of boundary conditions and that the Stern (1969) scenario requires vertical inhomogeneity to operate, if indeed it plays a role here.

3. Staircases as metastable equilibria

A second hypothesis for the formation of staircases from initially uniform T and S gradients is that permanent steps are induced by disturbances such as mechanical mixing or imposed flux imbalances. In this picture, staircases and statistically homogeneous salt fingering (such as that in Figs. 1b,c) both represent metastable equilibria. This notion is supported by the Stern and Turner (1969) experiments, described in the last

section, in which either uniform fingering or layers develop depending on initial conditions.

The metastable equilibrium hypothesis implies that the stepped structures observed in the laboratory represent true equilibria and that interface thicknesses would persist indefinitely at equilibrium values if the property jumps across them remained constant. In laboratory experiments to date the property jumps always decrease over time; thus the equilibrium thickness prediction has been tested only indirectly thus far. As property jumps run down, the interfaces generally broaden, linearly with t when fingering is vigorous (Stern and Turner 1969; Linden 1973; Taylor and Veronis 1996) and as $t^{1/2}$ when fingers are only marginally unstable (Taylor and Veronis 1996). In the former instance, the interface spreads at a speed that is at least an order of magnitude smaller than vertical velocities in the fingers (Linden 1973). A uniform spread rate is consistent with predictions which assume a critical Stern number and the so-called 4/3 law for solute flux (Stern and Turner 1969). This relatively slow rate of spread has been interpreted as evolution through a series of quasi equilibria (e.g., Stern and Turner 1969). Further evidence in favor of an equilibrium interface thickness is provided by the observation of Schmitt (1979) that interface spread can be reversed by replenishing the destabilizing property concentration in the upper layer.

The notion of an equilibrium interface thickness could be tested more directly by devising an experiment in which properties are extracted from the lower layer and replenished in the upper layer in such a manner that the property jumps are maintained.[4] Such maintenance is achievable in numerical simulations having periodic boundaries that allow the fluxes exiting the lower boundary to reenter from above. In an attempt to model an equilibrium interface, a numerical simulation was undertaken using the two-dimensional pseudospectral code described in MG. Parameters were $\sigma = 7$ and $\tau = 0.01$, characteristic of seawater, and $R_\rho = 2$. The computational domain height $L \approx 42d$, where $d \equiv (\nu\kappa_T/g\alpha T_z)^{1/4}$, was spanned by 1024 grid points and the width $L/2$ by 512 grid points. Initial conditions consisted of a step in T and S, with property jumps smoothed across five or so grid points according to a tanh profile. Small random perturbations to S were imposed.

As in similar experiments (Shen 1993), a series of fingers initially developed at the interface (Fig. 2a). The subsequent spread of the interface is compared against the spreading of a purely diffusive interface governed by

$$\Phi_t = \kappa_\Phi \Phi_{zz} \qquad (3.1)$$

with

$$\Phi(z, 0) = n\Phi_0, \qquad nL < z < (n + 1)L,$$

$$n = \cdots, -1, 0, 1, 2, \cdots \qquad (3.2)$$

The solution to (3.1)–(3.2) is

$$\Phi(z, t) = \frac{\Phi_0 z}{L} + \frac{\Phi_0}{\pi} \sum_{m=1}^{\infty} \frac{1}{m} \exp\left(-\kappa_\Phi \frac{4m^2\pi^2}{L^2} t\right) \sin\frac{2m\pi z}{L},$$
$$(3.3)$$

(Elliott and Tait 1977). Interface sharpness for the modeled T and S fields and for Φ was quantified as the integrated difference between the horizontally averaged fields and constant-gradient diffusive equilibria:

$$\Lambda_T(t) \equiv -\int_0^{L/2} [\langle T(z, t)\rangle - \overline{T}_z z] \, dz$$

$$+ \int_{L/2}^{L} [\langle T(z, t)\rangle - \overline{T}_z z] \, dz, \qquad (3.4)$$

$$\Lambda_S(t) \equiv -\int_0^{L/2} [\langle S(z, t)\rangle - \overline{S}_z z] \, dz$$

$$+ \int_{L/2}^{L} [\langle S(z, t)\rangle - \overline{S}_z z] \, dz, \qquad (3.5)$$

$$\Lambda_\Phi(t) \equiv -\int_0^{L/2} [\Phi(z, t) - \overline{\Phi}_z z] \, dz$$

$$+ \int_{L/2}^{L} [\Phi(z, t) - \overline{\Phi}_z z] \, dz, \qquad (3.6)$$

where $\overline{T}_z$, $\overline{S}_z$, and $\overline{\Phi}_z$ are the equilibrium gradients, and the brackets denote horizontal averages. The evolution of the two-dimensional salinity field and of $\langle T\rangle$ and $\langle S\rangle$ is depicted in Figs. 2 and 3. In Fig. 4, evolution of Λ_T and Λ_S is compared against that of Λ_Φ for different values of κ_Φ. Here T, S and Φ are scaled to have unit equilibrium gradients. Time is expressed in units of d^2/κ_T. Because initial Φ is a perfect step, Λ_Φ initially is slightly greater than Λ_T and Λ_S. For $t \lesssim 20$, the fingering interface spreads significantly faster than by thermal diffusion alone. However, by $t = 50$ the interface is decaying at much the same rate as a thermal diffusive interface. Similar results were reported by Shen (1989) for $\sigma = 1$, $\tau = 0.1$, and $R_\rho = 2$. [At such a rate, 10-m steps would decay on a timescale of order 6 months and 50-m steps on a timescale of order 15 years. In addition, steps would lose their "sharpness" on timescales an order of magnitude shorter (Elliott and Tait 1977).]

The failure of this numerical experiment to attain a layered equilibrium should not be weighed as evidence against the multiple equilibrium hypothesis because it

---

[4] More simply, one could examine the effect of layer depth, which determines the rate of run down, on the rate of interface spread.
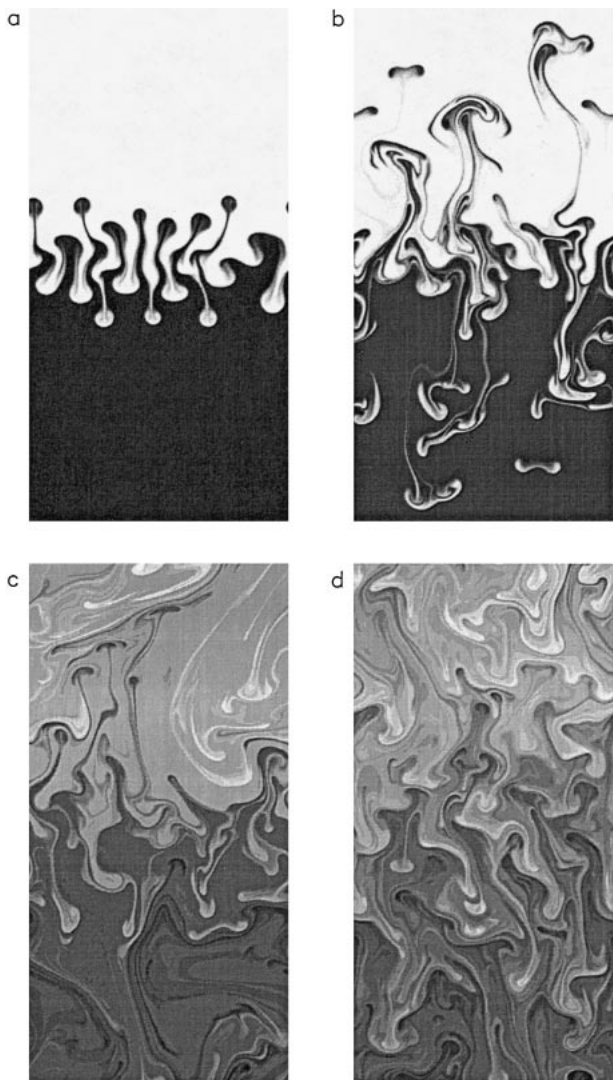
FIG. 2. Salinity field in a numerical simulation of fingers developing at an initially sharp interface for (a) $t = 6.13$, (b) $t = 9.19$, (c) $t = 12.25$, and (d) $t = 84.18$. In each frame, lighter shades represent higher salinities, and darker shades lower salinities.
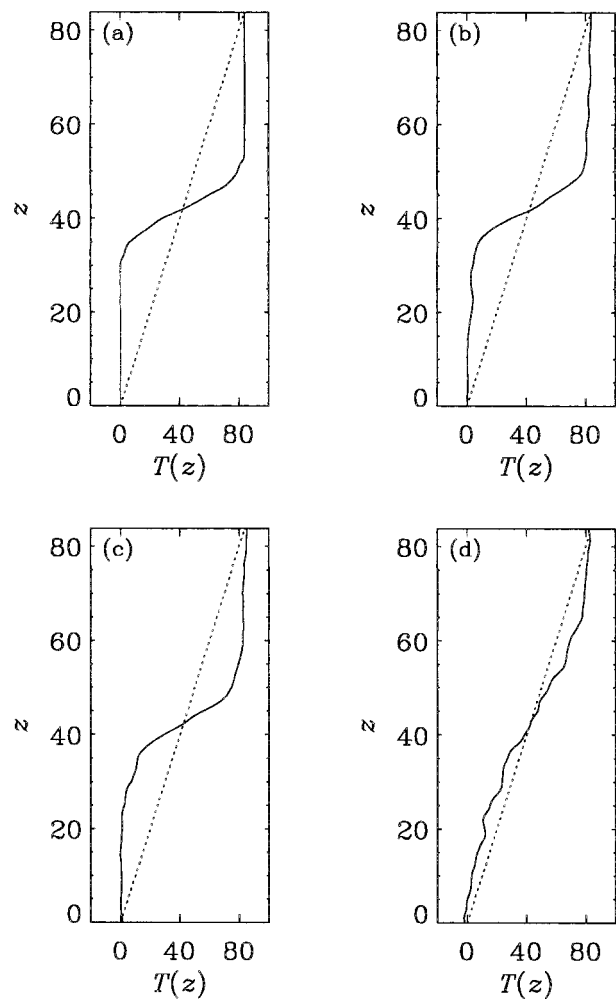

FIG. 3. Horizontally-averaged temperature in numerical simulation of fingers developing at an initially sharp interface, at the same times represented in Fig. 2: (a) $t = 6.13$, (b) $t = 9.19$, (c) $t = 12.25$, (d) $t = 84.18$. Instead of equilibrating at a finite thickness, the simulated interface decays toward a constant-gradient equilibrium, represented by the dashed lines. The interface sharpness measure Λ_T corresponds to the area between the dashed lines and solid curves.

is two-dimensional and samples only a single set of parameters. It does, however, suggest the existence of a criterion dividing conditions under which true layered equilibria arise (if indeed they do) and do not arise.

Finally, a particularly effective way to produce multiple layers in the laboratory is to impose an S flux from above onto a stable T gradient (Stern and Turner 1969; Schmitt 1997). Experiments in which a destabilizing S gradient is also present have not been reported. However, in the case of diffusive convection, layers develop in an analogous fashion when a T flux is applied from below, whether a destabilizing T gradient is present (Linden 1976) or not (Turner 1968). In the diffusive case, layer thicknesses have been shown to collapse to a function of R_ρ alone when scaled by $\kappa_T/\overline{N}$, where $\overline{N}$ is the buoyancy frequency of the mean stratification

(Kelley 1984). Such a relation has not yet been demonstrated for fingering staircases.

4. Negative density diffusion

Salt fingering has the distinctive property that, while vertical T and S fluxes are downgradient, vertical density flux is upgradient. This is because the potential energy released in transporting salt downward must exceed that expended in transporting heat upward, resulting in a net downward transport of mass.

Negative diffusion sharpens rather than smooths fluctuations. The negative diffusion of density associated with salt fingers thus suggests a means for generating and maintaining staircases (Schmitt 1994). This hy-
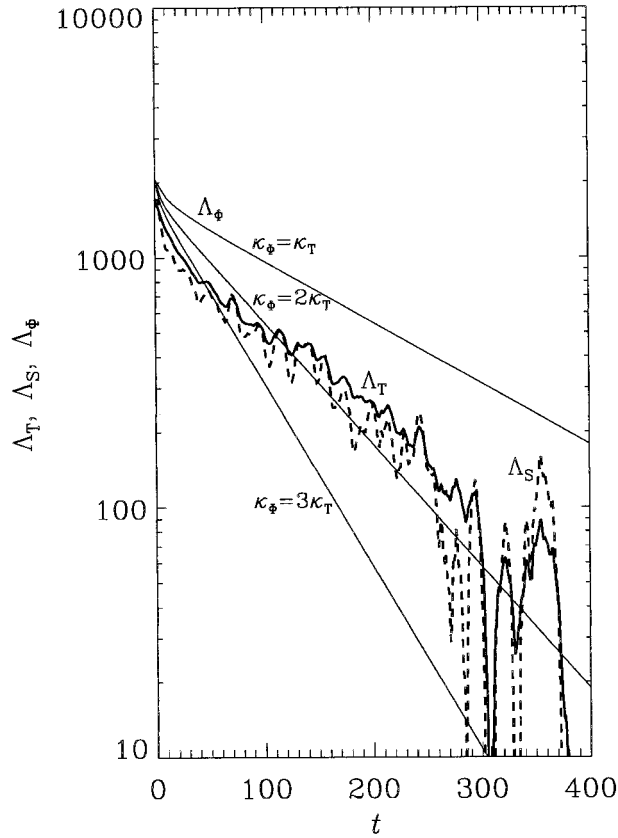
FIG. 4. Evolution of interface sharpness measures Λ_T, Λ_S, and Λ_Φ for temperature, salinity, and a hypothetical scalar Φ having diffusion coefficient κ_Φ. Thick solid curve: Λ_T; thick dashed curve: Λ_S; thin curves: Λ_Φ, for indicated κ_Φ. A boxcar filter 7 time units in width has been applied to Λ_T and Λ_S.

pothesis is evaluated with the aid of some numerical experiments below.

a. Diffusion equation for density

Suppose that salt fingering causes slow negative diffusion of density and convection more rapid positive diffusion. The influence of fingering on horizontal-mean density ρ (averaged laterally over many finger widths) can then be represented by a simple one-dimensional diffusion equation,

$$\rho_t = (K_\rho \rho_z)_z, \qquad (4.1)$$

where z is the vertical coordinate and K_ρ is an effective vertical diffusion coefficient specified by

$$K_\rho = K_\rho^f = -0.1 \text{ cm}^2 \text{ s}^{-1},$$

$$\rho_z < 0 \quad \text{(fingering)}, \qquad (4.2)$$

$$K_\rho = K_\rho^c = 1000 \text{ cm}^2 \text{ s}^{-1},$$

$$\rho_z \geq 0 \quad \text{(convection)}. \qquad (4.3)$$

The value assigned to the negative fingering diffusivity

K_ρ^f is comparable to estimates based on microstructure measurements and numerical simulations[5] and is large enough to overcome the estimated smoothing effects of intermittent turbulence (Schmitt 1994). The large value assigned to the positive convective diffusivity K_ρ^c reflects the assumption that convective mixing occurs very rapidly compared to mixing by salt fingers. The results are insensitive to its exact value, provided $K_\rho^c \gg |K_\rho^f|$.

Equations (4.1)–(4.3) were solved numerically using an implicit finite difference scheme,

$$\rho_i^{n+1} = \rho_i^n + \frac{\Delta t}{(\Delta z)^2} [\kappa_{\rho, i+(1/2)}^n (\rho_{i+1}^{n+1} - \rho_i^{n+1})$$

$$- \kappa_{\rho, i-(1/2)}^n (\rho_i^{n+1} - \rho_{i-i}^{n+1})], \quad (4.4)$$

where superscripts denote time levels, subscripts denote grid points, and Δt and Δz denote time step and grid spacing. One hundred grid points were employed, with $\Delta z = 20$ cm and $\Delta t = 400$ s. Boundary conditions were periodic (modulo the density contrast across the domain), which required inverting a cyclic tridiagonal system at each time step. Initial conditions consisted of small-amplitude random noise superimposed on a uniform stable ρ gradient. Subsequent evolution of $\rho(z, t)$ for a particular realization of initial conditions is shown in Fig. 5. Other realizations are qualitatively similar. Initially, the density fluctuations are minute. Because of negative diffusion, the fluctuations amplify, giving rise to numerous density inversions. Convection rapidly mixes across the inversions, yielding density steps between adjacent grid cells. Smaller steps weaken and merge successively with larger ones until a single step spans the entire domain. Merging occurs because layers having larger density jumps below than above transport more mass across the steeper density interface below than they receive from above. Density thus decreases until the layer merges with the one above it. (It should be noted that this process depends upon grid spacing because the upgradient density flux across a jump $\Delta\rho$ spanning one grid cell is $K_\rho^f \Delta\rho/\Delta z$. Reducing Δz increases the upgradient fluxes and speeds the merging processes.) Although having a fixed interface thickness and flux proportional to $\Delta\rho$ seems artificial, such behavior is not unlike that of laboratory salt fingering interfaces, whose thicknesses are relatively insensitive

---

[5] In terms of effective salt diffusivity K_S and temperature diffusivity K_T, $K_\rho = (R_\rho K_T - K_S)/(R_\rho - 1)$ (Shen 1995). On the basis of microstructure measurements, Schmitt (1988) estimates effective salt diffusivities of 0.28 to 0.74 cm² s⁻¹ (assuming buoyancy flux ratio $\alpha K_T T_z / \beta K_S S_z \approx 0.5$) for fingering interfaces in the western tropical North Atlantic ($R_\rho \approx 1.6$). These estimates are based on ratios of flux to mean gradient averaged over layers and interfaces, however. In the present context, what is needed is the ratio of flux to gradient within an interface. The latter is roughly ten times the mean gradient, implying $K_S \approx 0.03$ to 0.07 cm² s⁻¹, and $K_\rho \approx -0.02$ to -0.06 cm² s⁻¹. Merryfield and Grinder, in numerical simulations of heat/salt fingers in an infinitely thick interface, find $K_\rho \approx -0.13$ cm² s⁻¹ at $R_\rho = 1.5$.
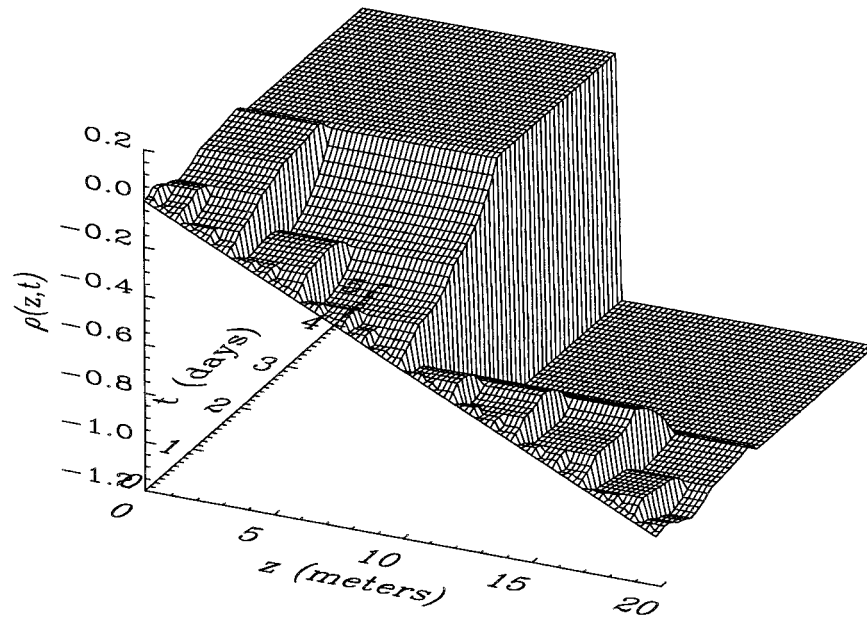
FIG. 5. Evolution of density $\rho(z, t)$ from small fluctuations imposed on an initially uniform gradient, according to negative diffusion equations (4.1)–(4.3). Density is expressed in arbitrary units.

to salinity jump ΔS, scaling as $(\beta\Delta S)^{-1/3}$ (Stern and Turner 1969; Linden 1973). Similarly, fingering salt fluxes at a fixed R_ρ are often cited as following $\beta F_S \propto (\beta\Delta S)^{4/3}$ (e.g., Schmitt 1979; Taylor and Bucens 1989), which is not too different from $F_\rho \propto \Delta\rho$.

The results shown in Fig. 5 superficially appear to support the notion that negative density diffusion is responsible for staircases. However, at least two considerations cast doubt on this interpretation. The first is that the physical scale of the steps increases with time and is limited only by the height of the computational domain. Thus there is no obvious mechanism for establishing a preferred scale. The second is that (4.1)–(4.3) do not provide a consistent description of the mixing process. This is because countergradient transport of ρ is a consequence of the combined transports of T and S, which should be treated separately. Such a treatment is considered next.

b. Diffusion equations for temperature and salinity

Consider horizontal-mean T and S, which are governed by

$$T_t = (K_T T_z)_z, \tag{4.5}$$

$$S_t = (K_S S_z)_z, \tag{4.6}$$

and together determine horizontal-mean density through

$$\rho = \rho_0[1 - \alpha(T - T_0) + \beta(S - S_0)], \tag{4.7}$$

where T_0, S_0 and ρ_0 denote constant reference values and a linear equation of state is assumed. Equations (4.5)–(4.7) were solved using

$$K_S = K_S^f = 0.2 \text{ cm}^2 \text{ s}^{-1}, \qquad K_T = K_T^f = 0.08 \text{ cm}^2 \text{ s}^{-1},$$

$$\rho_z < 0 \quad \text{(fingering)}, \tag{4.8}$$

$$K_S = K_S^c = 1000 \text{ cm}^2 \text{ s}^{-1}, \qquad K_T = K_T^c = 1000 \text{ cm}^2 \text{ s}^{-1},$$

$$\rho_z \geq 0 \quad \text{(convection)}, \tag{4.9}$$

where K_S^f and K_T^f have been assigned values similar to those found in a $R_\rho = 1.5$ numerical simulation (MG). When initial T, S consist of small fluctuations about uniform gradients, large-amplitude steps did not spontaneously arise. Convective layers did form when departures from uniform gradients were sufficiently large because of the more rapid decay of S fluctuations than T fluctuations. The scale of these layers is determined by that of the imposed disturbances. A sequence of layers such as a staircase thus might be generated by a train of internal waves, although one would need to show how such a process could produce coherent steps hundreds of kilometers in lateral extent. Zhurbas et al. (1987) obtained similar results using R_ρ-dependent K_T and K_S. They suggested that regular disturbances in T and S might be produced by thermohaline intrusions (see sec. 5), but made no attempt to account for crucial lateral advection effects.

5. Staircases as intrusions

This section develops the hypothesis that thermohaline staircases arise from double-diffusive intrusions. Such a connection was proposed by Zhurbas and Ozmidov (1983), who found that steps in the C-SALT region develop T and S inversions near their peripheries.

After a brief review of some properties of intrusions, linear and nonlinear calculations are presented which support this hypothesis. Observational evidence is then discussed.

a. Nature of intrusions

Salt fingers occur because diffusive transport of T exceeds that of S. However, salt fingers themselves transport S more effectively than T, and this unequal transport, in conjunction with lateral T and S gradients, gives rise to inclined, fingerlike intrusions. Stability when vertical T and S gradients favor fingering and lateral T and S gradients are density-compensating has been explored by Stern (1967), Toole and Georgi (1981), McDougall (1985), Niino (1986), and Walsh and Ruddick (1995, 2000). Kuzmina and Rodionov (1992) and May and Kelly (1997) consider the influence of baroclinicity. Under oceanic conditions, predicted vertical wavelengths are of order tens of meters, and slopes are less than one degree or so from horizontal. A distinctive feature of intrusions driven by salt fingering is that warm and salty intrusions rise across isopycnals, whereas cool and fresh intrusions sink.

Because double-diffusive intrusions grow most rapidly where lateral T and S gradients are large, they are expected to be most conspicuous at fronts. Observations show that many fronts indeed harbor intrusive features (e.g., Gregg 1975; Horne 1978; Ruddick 1992), although intrusions have also been found where lateral gradients are spatially extended (Rudels et al. 1999).

A somewhat standard characterization of fully developed intrusions is that they feature prominent T and S inversions so that regions of salt fingering (T and S increasing upward) alternate in depth with regions of diffusive convection (T and S increasing downward).

b. Linear theory

In this subsection, linear theory is employed to argue that conventional intrusions featuring prominent T and S inversions are not the only possible outcome of intrusive instability and that staircaselike configurations as are possible as well. A criterion dividing these two outcomes is derived. As in recent studies by Walsh and Ruddick (1995, 1998, 2000, henceforth WR95, WR98, WR00, respectively), attention is focused on effects of R_ρ-dependent fingering fluxes and turbulent mixing, whereas effects of rotation are excluded. This can partially be justified by the fact that rotation does not affect the growth rate, wavelength, or cross-front slope of the fastest-growing intrusions (McDougall 1985; Kerr and Holyer 1986). Such modes also have vanishing alongslope velocity, but do possess an alongslope component of slope when rotation is accounted for. Baroclinic effects (Kuzmina and Rodionov 1992; May and Kelly 1997) are also excluded.

To motivate the discussion, consider the initial development of intrusions at a particular horizontal location. Assuming that initial gradients are uniform and that a single Fourier mode dominates, temperature and salinity evolve according to

$$T(x_0, z, t) = \overline{T}_z z + \hat{T} e^{imz+\lambda t}, \qquad (5.1)$$

$$S(x_0, z, t) = \overline{S}_z z + \hat{S} e^{imz+\lambda t}, \qquad (5.2)$$

where m is vertical wavenumber, λ is growth rate, $\hat{T}$ and $\hat{S}$ are the (possibly complex) intrusion amplitudes (e.g., Toole and Georgi 1981), and $\overline{T}_z$ and $\overline{S}_z$ are the background vertical gradients.

It is convenient to represent this evolution on the $(\alpha T_z, \beta S_z)$ plane as in Fig. 6, where approximate boundaries dividing regions of salt fingering, convection, diffusive convection and stability are indicated. Initial amplitudes are assumed arbitrarily small, so (5.1)–(5.2) represent essentially a point on this plane (Fig. 6a). As the intrusions develop, (5.1)–(5.2) describe line segments having a slope $(\alpha\hat{T}/\beta\hat{S})^{-1}$ (Fig. 6b), which must be <1 for intrusions to grow. If (T, S) continue to be described by their linear eigenfunctions, one of two possible developments must occur. The first, labeled "I," is that S_z reverses sign before T_z and a portion of the intrusion becomes stable (Fig. 6c). At still later times, T_z also reverses sign, and intrusions consist of a cyclical arrangement of fingering, stable, diffusively convective, stable, and fingering layers (Fig. 6d). The second possible development, labeled "S," is that evolution occurs toward $\alpha T_z = \beta S_z$, the locus of neutral stability to convection (Fig. 6b). At later times this criterion is exceeded (Figs. 7c,d), and intrusions consist of alternating fingering and convective layers—a thermohaline staircase.

It remains to establish whether evolution toward staircase configurations can be realized. Referring again to Fig. 6, growing intrusions governed by (5.1)–(5.2) will evolve toward staircases if

$$\alpha\hat{T}/\beta\hat{S} > \alpha\overline{T}_z/\beta\overline{S}_z \equiv \overline{R}_\rho. \qquad (5.3)$$

Is it straightforward to express this criterion in terms of system parameters. The linearized equations governing small departures T and S from a state of uniform T and S gradients and no motion are

$$T_t + u\overline{T}_x + w\overline{T}_z = -F_z^{(T)}, \qquad (5.4)$$

$$S_t + u\overline{S}_x + w\overline{S}_z = -F_z^{(S)}, \qquad (5.5)$$

(WR95) where u and w are horizontal and vertical velocity and $F^{(T)}$ and $F^{(S)}$ are vertical diffusive fluxes of temperature and salt. (The momentum equations need not be considered here.) The fluxes are assumed, as in WR00, to consist of R_ρ-dependent fingering contributions, which differ for T and S, together with a turbulent flux that mixes T and S equally:

$$F^{(T)} = -[K_T^f(R_\rho) + K_{\text{turb}}]T_z, \qquad (5.6)$$

$$F^{(S)} = -[K_S^f(R_\rho) + K_{\text{turb}}]S_z, \qquad (5.7)$$

where K_T^f and K_S^f are effective fingering diffusivities for
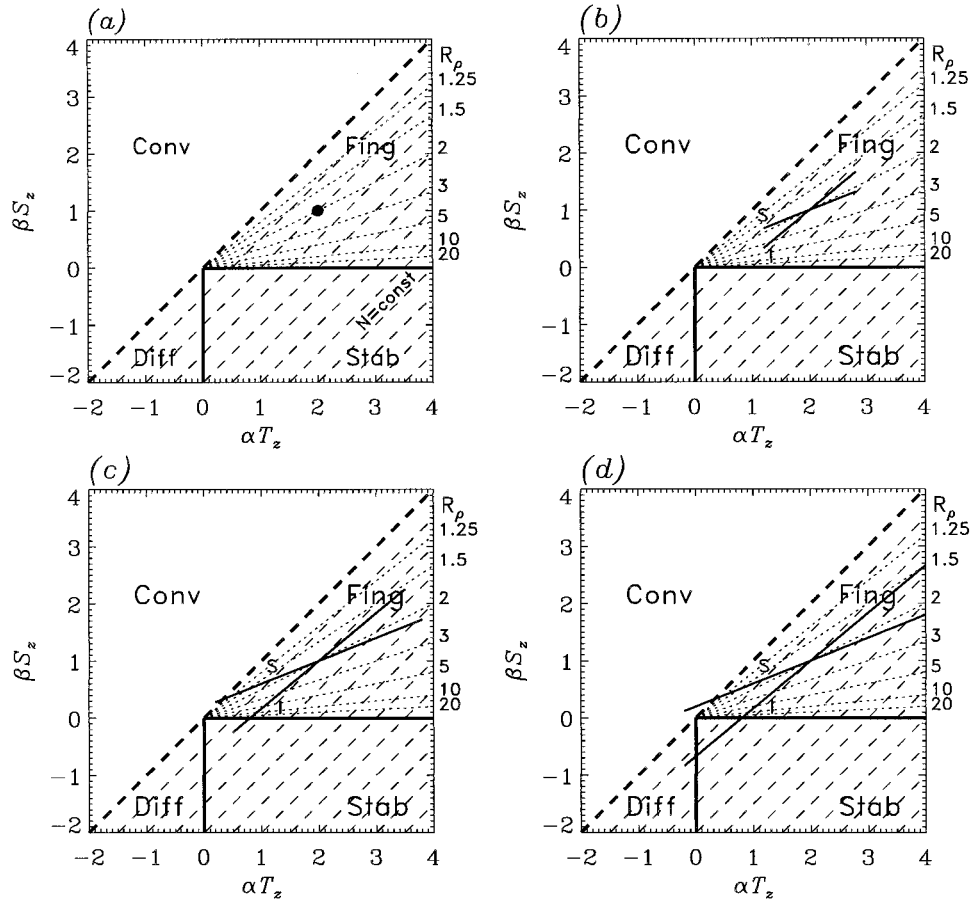
FIG. 6. Schematic depiction of intrusion growth on the $(\alpha T_z, \beta S_z)$ plane, according to (5.1)–(5.2). Long-dashed lines denote constant N, and short-dashed lines constant R_ρ. Heavy lines separate fingering, convective, diffusive convective and stable regimes. (a) Initial conditions, lying close to background gradients, are denoted by the dot. (b) Growing intrusions describe line segments which lengthen in time. A line segment whose slope is less than R_ρ^{-1} is labeled by "S," and one whose slope is greater than R_ρ^{-1} is labeled by "I." (For intrusions to grow, this slope must lie between 0 and 1.) (c) As growth continues, I begins to penetrate the stable regime, and S the convective regime. (d) Still later, I penetrates the diffusive–convective regime as well. Intrusion I then consists of sequences of fingering, stable, diffusive convective, convective and fingering layers, whereas S consists of alternating fingering and convective layers.

T and S, and K_{turb} is an effective turbulent diffusivity. The fingering diffusivities are related by $K_T^f = \gamma_f K_S^f / R_\rho$, where flux ratio γ_f is a relatively slowly varying function of R_ρ, taken to be constant. Substituting (5.6)–(5.7) into (5.4)–(5.5) and considering perturbations $(T, S) = (\hat{T}, \hat{S})e^{ikx+imz+\lambda t}$ yields

$$[\lambda + m^2(\gamma_f K_S' + K_{\text{turb}})]\alpha\hat{T} + m^2\gamma_f(K_S^f - K_S'\overline{R}_\rho)\beta\hat{S}$$

$$= i(m\alpha\overline{T}_x - k\alpha\overline{T}_z)\hat{\psi}, \qquad (5.8)$$

$$-m^2K_S'\alpha\hat{T} + [\lambda + m^2(K_S^f + K_S'\overline{R}_\rho + K_{\text{turb}})]\beta\hat{S}$$

$$= i(m\beta\overline{S}_x - k\beta\overline{S}_z)\hat{\psi}, \qquad (5.9)$$

where K_S' is the derivative of K_S^f with respect to R_ρ, $\hat{\psi}$ is streamfunction, for which $(u, w) = (-\hat{\psi}_z, \hat{\psi}_x)$, and K_S and K_S' are evaluated at $\overline{R}_\rho$. Straightforward evaluation of $\alpha\hat{T}/\beta\hat{S}$ from (5.8)–(5.9) and substitution into (5.3)

yields the proposed criterion for evolution of intrusions into thermohaline staircases:

$$\lambda < \frac{m^2 K_S^f(\overline{R}_\rho)}{\overline{R}_\rho - 1}\left[(1 - \gamma_f) - \frac{s}{\Gamma_S}(\overline{R}_\rho - \gamma_f)\right.$$

$$\left. - \frac{K_{\text{turb}}}{K_S^f(\overline{R}_\rho)}(\overline{R}_\rho - 1)\right], \qquad (5.10)$$

where $\Gamma_S \equiv \overline{S}_x/\overline{S}_z$ is the background isohaline slope, and $s \equiv k/m$, the cross-frontal intrusion slope, is positive for growing intrusions.

Implications of (5.10) are now examined. In this discussion, density ratio $\overline{R}_\rho$ and turbulent mixing coefficient K_t, which depend upon local conditions, are allowed to vary. The buoyancy flux ratio for fingering is set to $\gamma_f = 0.6$, a value fairly well constrained by lab-
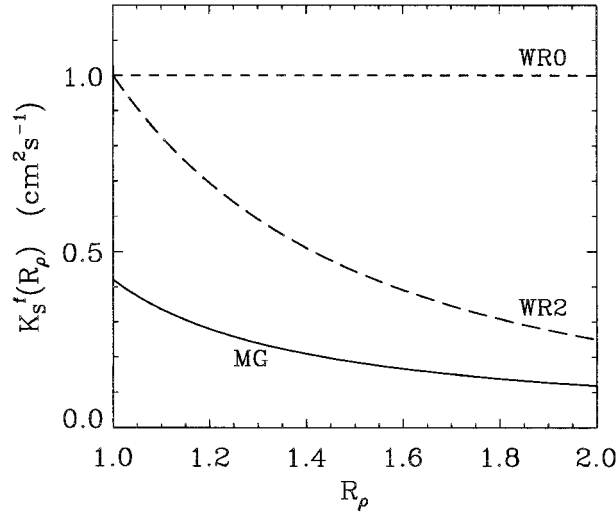
FIG. 7. Functional forms considered for $K_S^f(R_\rho)$, the effective vertical salt diffusivity due to salt fingering.

FIG. 8. Example of the dependence on R_ρ of λ, the intrusion growth rate and rhs of (5.10). Intrusions evolve toward staircase configurations when $\lambda <$ rhs, which occurs when R_ρ is less than a critical value R_ρ^{stair}, which in this instance ≈ 1.12. Parameters: WR0 flux law, $\Gamma_S = 5 \times 10^{-4}$, $K_{\text{turb}} = 0.1$ cm² s⁻¹, Pr given by (5.11). The vertical axis is labeled in units of buoyancy frequency N.

oratory and numerical experiments (e.g., Schmitt 1979; MG). In specifying $K_S^f(R_\rho)$, three functional forms are considered (Fig. 7). The first two are based on the ad hoc formula $K_S^f(R_\rho) = K_{\text{max}} R_\rho^{-n_f}$ of WR98, choosing $K_{\text{max}} = 1$ cm² s⁻¹ and $n_f = 0$ (case WR0) or $n_f = 2$ (WR2). The third form is obtained from the Merryfield and Grinder simulations of salt fingering subject to uniform background gradients: $K_S^f = 0.17(1 - \tau R_\rho)/(R_\rho - \gamma_f)$ cm² s⁻¹ (case MG). The growth rate λ is determined by m, s and the parameters through a linear eigenvalue problem (WR00). When the fastest-growing mode is considered, m and s acquire specific values. Finally, the effective Prandtl number, $\text{Pr} \equiv A(\overline{R}_\rho)/[K_S^f(\overline{R}_\rho) + K_{\text{turb}}]$ where A is effective viscosity, appears in the linear eigenvalue problem. The proper choice for this parameter is not well known, and a range of choices is thus considered. Following Ruddick (1985), WR98 take momentum flux to be proportional to the fingering buoyancy flux plus a turbulent flux so that

$$\text{Pr} = \text{Pr}_0\left(\frac{1 - \gamma_f}{R_\rho - 1}K_S^f(\overline{R}_\rho) + K_{\text{turb}}\right)$$
$$\div (K_S^f(\overline{R}_\rho) + K_{\text{turb}}), \quad (5.11)$$

with $\text{Pr}_0 = 10$. Conversely, laboratory experiments of Ruddick et al. (1989) suggest that fingering does little to enhance viscous stress. Assuming that viscous stress is enhanced by turbulence alone implies

$$\text{Pr} = \frac{\text{Pr}_0 K_{\text{turb}} + \nu}{K_S^f(\overline{R}_\rho) + K_{\text{turb}}}, \quad (5.12)$$

where the molecular viscosity $\nu \approx 0.01$ cm² s⁻¹ has been introduced to ensure a physical lower bound.

Several properties of criterion (5.10) merit discussion.

1) Staircases tend to be favored at low values of R_ρ because the right-hand side of (5.10) increases more
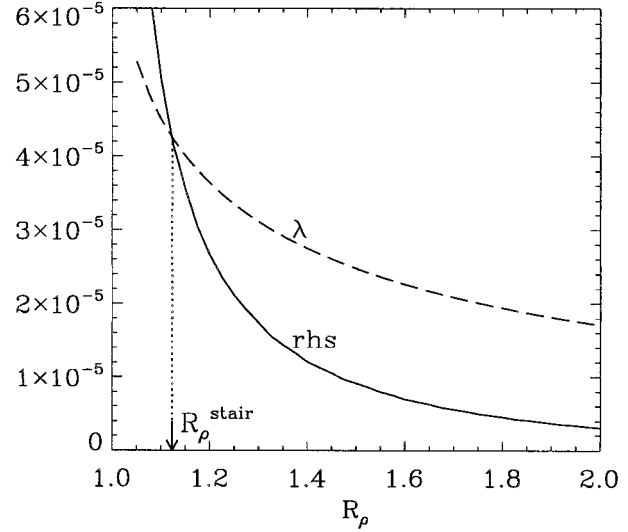
rapidly than growth rate λ as $R_\rho \to 1$. This tendency is illustrated in Fig. 8, where λ and the right-hand side of (5.10) are plotted against R_ρ for K_S^f given by WR0, $K_{\text{turb}} = 0.01$ cm² s⁻¹, Pr given by (5.11) with $\text{Pr}_0 = 10$, and m and s characterizing the fastest-growing mode. According to criterion (5.10), staircases are favored when R_ρ is less than a critical value R_ρ^{stair}, which in this instance is about 1.12.

2) Staircases are favored by a low turbulent mixing coefficient K_{turb}. Figure 9 illustrates how the predicted threshold R_ρ^{stair} varies with K_{turb} for K_S^f given by WR0 (solid curves) and WR2 (dashed curves), with Pr specified by (5.11) (thick curves) and (5.12) (thin curves). In each instance, threshold R_ρ^{stair} grows larger as K_{turb} decreases.

3) Threshold R_ρ^{stair} is considerably larger when salt fingering is presumed not to contribute to viscous stress, so that Pr is specified by (5.12). For example, for flux law WR2 and $K_{\text{turb}} = 0.01$ cm² s⁻¹ (Fig. 9a), R_ρ^{stair} increases from 1.08 when Pr is specified by (5.11) to 1.44 when Pr is specified by (5.12), assuming $\text{Pr}_0 = 10$. For (5.11) and flux law MG, (5.10) is not satisfied for any $\text{Pr}_0 \geq 1$, $R_\rho > 1$.

4) Threshold R_ρ^{stair} becomes still larger as the coefficient Pr_0 in (5.12) decreases from 10 to 1 (Fig. 9b).

5) Criterion (5.10) tends to be satisfied for sufficiently large m even when it is not for the fastest-growing mode. In Fig. 10, contours depict linear growth rate versus m and s. Values of (m, s) where evolution is toward staircases are indicated by "+" and values where evolution is toward conventional intrusions are indicated by "−." With $R_\rho = 1.1$, flux law WR2 and Pr given by (5.12) with $\text{Pr}_0 = 10$, (5.10) is
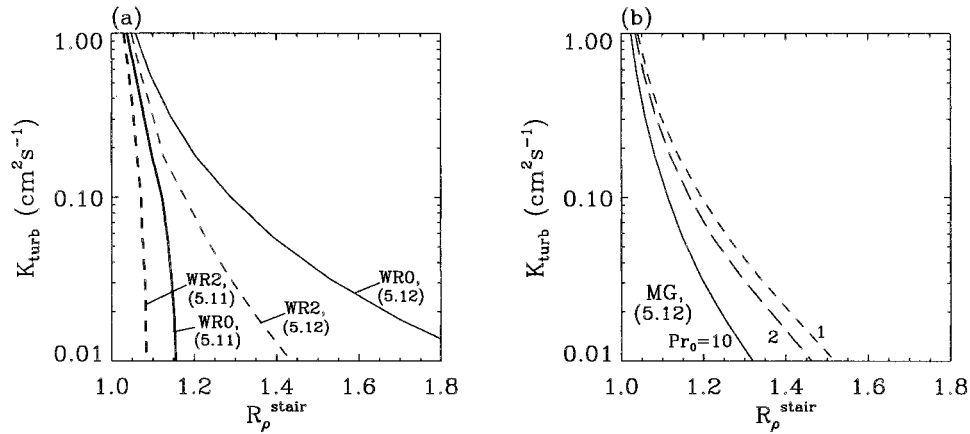
FIG. 9. Critical value R_ρ^{stair}, below which staircases form, as a function of K_{turb} for (a) flux laws WR0 and WR2, Pr given by (5.11) and (5.12) and $\text{Pr}_0 = 10$, and (b) flux law MG, Pr given by (5.12) with $\text{Pr}_0 = 10$, 2, and 1.

satisfied for the fastest-growing mode (Fig. 10a). For $R_\rho = 1.6$, the fastest-growing mode evolves toward conventional intrusions, but modes having comparable s and $m \gtrsim 30\%$ larger evolve toward staircases (Fig. 10b).

6) Criterion (5.10) is independent of Γ_S provided $s \ll 1$ because λ, s, and m^2 are then proportional to Γ_S (see appendix).

7) In the limit of large Prandtl number, $\alpha\hat{T}/\beta\hat{S}$ can be obtained analytically (McDougall 1985; WR95). When $K'_S = 0$ and $K_{\text{turb}} = 0$, this leads to $R_\rho^{\text{stair}} = 1 + \gamma/3$, or $R_\rho^{\text{stair}} = 1.133$ when $\gamma = 0.6$.

c. Nonlinear calculations

In the preceding subsection, linear theory was employed to determine the conditions under which intrusions evolve toward staircase configurations rather than toward conventional intrusions. To assess whether these tendencies are realized in equilibrated intrusions, nonlinear calculations are needed.

Equilibration of intrusions has been examined previously by WR98, who solved the nonlinear equations of motion in a tilted reference frame aligned with the intrusions. Because the ambient T and S gradients were assumed uniform, the governing equations of WR98 depend only on the spatial coordinate normal to the intrusions. All numerical solutions shown by WR98 equilibrated as conventional intrusions. This is not in contradiction with the present results, as discussed below.

1) FORMULATION

The approach adopted here for computing the nonlinear evolution of intrusions is similar to that of WR98, although the equations solved and numerical method employed are different. As a starting point, consider the Boussinesq equations of motion in two dimensions,

$$\nabla^2\psi_t + J(\psi, \nabla^2\psi) = -T_x + S_x + (A\psi_{xz})_{xz}$$
$$+ (A\psi_{zz})_{zz}, \qquad (5.13)$$

$$T_t + J(\psi, T) = (K_T T_z)_z, \qquad (5.14)$$

$$S_t + J(\psi, S) = (K_S S_z)_z, \qquad (5.15)$$

together with equation of state (4.7). Here ψ is streamfunction, defined as in section 5b, and $J(\psi, \cdot) = \psi_x \partial_z - \psi_z \partial_x$ is the Jacobian operator. Time has been expressed in units of inverse buoyancy frequency $\overline{N}^{-1}$ of the undisturbed state, diffusivity in units of $K_{\text{max}} = 1.0$ cm^2 s^{-1}, length in units of $d \equiv (K_{\text{max}}/\overline{N})^{1/2}$, temperature in units of $\overline{N}^2 \, d/g\alpha$, and salinity in units of $\overline{N}^2 \, d/g\beta$. The effective viscosity A, like K_T and K_S, is assumed to operate on vertical gradients only.

To complete (5.13)–(5.15), effective viscosity A and diffusivities K_S and K_T must be specified as functions of the vertical gradients of temperature and salinity. In a nonlinear calculation, vertical gradients may depart from the fingering regime, and transports under convective, diffusive convective and stable conditions must be specified as well. These transports are somewhat uncertain, and the functional forms suggested by WR98 are adopted here (Table 1), except in instances where cases MG for fingering diffusivities and (5.12) for fingering-regime viscosity are considered.

Two-dimensional equations (5.13)–(5.15) were solved using a pseudospectral algorithm much like that described in MG. Such computations pose significant challenges because the growing intrusions are subject to convective and stratified-shear instabilities, which excite motions on temporal and spatial scales much smaller than those of the intrusions. By using very high resolution together with hyperviscosity and hyperdiffusion to damp the smallest scales, numerically stable solutions were obtained. However, because of the significant computing resources required, it was not feasible to follow many such runs to equilibrium. In addition, explicit con-
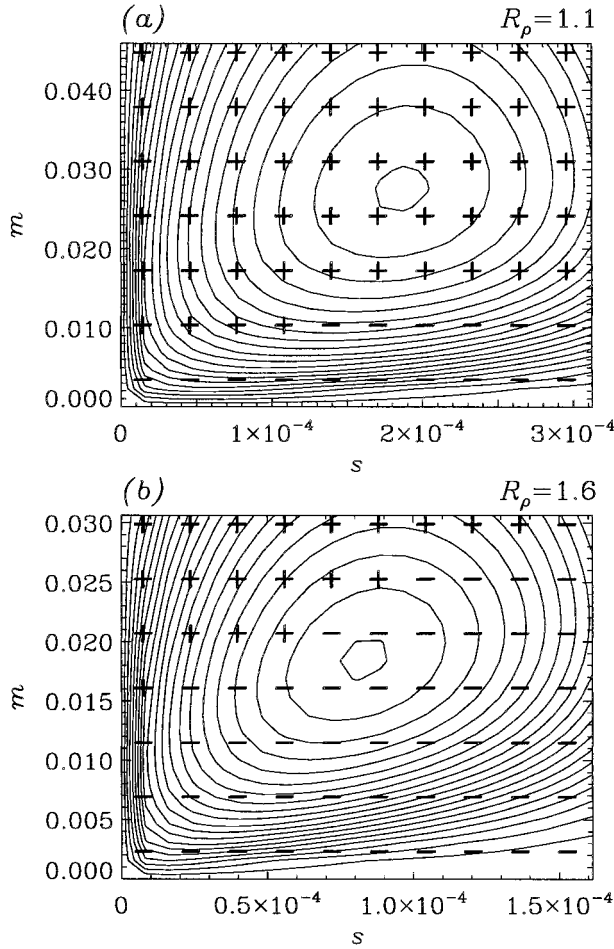
FIG. 10. Linear growth rate (units of N) as a function of intrusion slope s and dimensionless vertical wave number m (units of $[K_{max}/N]^{1/2}$). Plus signs indicate where criterion (5.10) for evolution toward staircases is satisfied. Minus signs indicate where evolution is toward conventional intrusions. In both cases, $K_{turb} = 0.01$ cm^2 s^{-1}, $\Gamma_S = 5 \times 10^{-4}$ and the WR2 flux law is employed, with Pr given by (5.12) and Pr$_0 = 10$: (a) $R_\rho = 1.1$, maximum growth rate 2.66 $\times$ 10^{-4}; fastest-growing mode evolves toward a staircase; (b) $R_\rho = 1.6$, maximum growth rate 0.75 $\times$ 10^{-4}; fastest-growing mode evolves toward conventional intrusions.

vective and gravity-wave motions complicate the interpretation of these runs. Therefore, results of these computations are not described here. Instead, a one-dimensional problem was solved, as described below.

Consider a coordinate system (χ, ζ) that is rotated with respect to (x, z) by $-\theta$, where $\theta = -\tan^{-1}s$ (Fig. 11). Equations (5.13)–(5.15) can be expressed with respect to the new coordinates by applying the transformation

$$\partial_x = \cos\theta \, \partial_\chi - \sin\theta \, \partial_\zeta, \qquad (5.16)$$

$$\partial_z = \sin\theta \, \partial_\chi + \cos\theta \, \partial_\zeta. \qquad (5.17)$$

If ambient T and S gradients are uniform so that intrusions are invariant with respect to the along-intrusion coordinate χ, (5.13)–(5.15) become

$$Z_t = -\sin\theta(T - S)_\zeta + \cos^2\theta(AZ)_{\zeta\zeta}, \qquad (5.18)$$

$$T_t = -U(\overline{T}_x \cos\theta + \overline{T}_z \sin\theta) + \cos^2\theta(K_T T_\zeta)_\zeta, \qquad (5.19)$$

$$S_t = -U(\overline{S}_x \cos\theta + \overline{S}_z \sin\theta) + \cos^2\theta(K_S S_\zeta)_\zeta, \qquad (5.20)$$

where $Z = \psi_{\zeta\zeta}$ is vorticity, $U = -\psi_\zeta$ is along-intrusion velocity, and

$$\overline{T}_x = \frac{\Gamma_S}{R_\rho - 1}, \qquad \overline{T}_z = \frac{R_\rho}{R_\rho - 1}, \qquad (5.21)$$

$$\overline{S}_x = \frac{\Gamma_S}{R_\rho - 1}, \qquad \overline{S}_z = \frac{1}{R_\rho - 1} \qquad (5.22)$$

are the background gradients. As throughout this paper, it is assumed that horizontal temperature and salinity gradients are density compensating.

For each choice of parameters, slope s is that of the fastest-growing mode, and the range in ζ of the computational domain is equal to the wavelength of the fastest-growing mode. Boundary conditions with respect to ζ are periodic, and (5.18)–(5.22) are solved numerically by means of a Fourier pseudospectral scheme, with dealiasing according to the 2/3 rule (Canuto et al. 1988). Between 64 and 512 Fourier modes are considered, as dictated by requirements of resolution. Initial conditions consist of density compensating perturbations to T and S, constructed by assigning Gaussian-distributed random values to the Fourier coefficients and scaling by inverse wavenumber squared. The initial perturbations were assigned dimensionless variances of 10^{-2}.

2) RESULTS

The nonlinear evolution of intrusions is in accord with tendencies deduced from linear theory: in all instances considered, intrusions equilibrated as staircases when criterion (5.10) was satisfied and as conventional intrusions when it was not. An example is shown in Fig. 12, where the critical value R_ρ^{stair} dividing staircase and conventional-intrusion regimes is traced by the heavy curve. Flux law MG and Pr given by (5.12) with Pr$_0 = 1$ are considered, and ambient conditions are characteristic of the C-SALT region (except for R_ρ; see Table 2). When (R_ρ, K_{turb}) lies to the left of this curve, the numerical solutions equilibrate as staircases (filled circle; inset a). Conventional intrusions are realized to the right of this curve (open circles; insets b, c, d).

A notable feature of the numerical solutions is that for staircases the along-intrusion velocity $U(\zeta)$ consists of pairs of narrow, oppositely directed jets centered on the fingering interface (Fig. 12, inset a). The resultant shear, coupled with along-intrusion property variations, maintains the sharp interfacial T and S gradients. This is in marked contrast to conventional intrusions for which $U(\zeta)$ has broad extrema nearly spanning the depth range of each intrusion (Fig. 12; inset b).

The development of laminae in staircases and con-

Table 1. Specification of effective diffusivities K_S and K_T and effective viscosity A (units of cm^2 s^{-1}). In all cases $\gamma_f = 0.6$ and $\gamma_d = 0.2$.

	Salt fingering $\rho_z < 0,\ 1 < R_\rho < \infty$	Diffusive convection $\rho_z < 0,\ 0 < R_\rho < 1$	Stable $\rho_z < 0,\ R_\rho < 0$	Convection $\rho_z \geq 0$
K_S^ζ (WR0)	1			
K_S^ζ (WR2)	R_ρ^{-2}			
K_S^ζ (MG)	$0.17\dfrac{1 - \tau R_\rho}{R_\rho - \gamma_f}$			
K_S	$K_S^\zeta + K_{\mathrm{turb}}$	$\gamma_d R_\rho K_T^d + K_{\mathrm{turb}}$	K_{turb}	K_{conv}
K_T^d (WR0)		1		
K_T^d (WR2)		R_ρ^{-3}		
K_T^d (MG)		R_ρ^{-3}		
K_T	$\gamma_f K_S^\zeta/R_\rho + K_{\mathrm{turb}}$	$K_T^d + K_{\mathrm{turb}}$	K_{turb}	K_{conv}
A (5.11)	$\mathrm{Pr}_0\left(\dfrac{1 - \gamma_f}{R_\rho - 1}K_S^\zeta + K_{\mathrm{turb}}\right)$	$\mathrm{Pr}_0\left(\dfrac{1 - \gamma_d}{1 - R_\rho}K_T^d + K_{\mathrm{turb}}\right)$	$\mathrm{Pr}_0 K_{\mathrm{turb}}$	$\mathrm{Pr}_0 K_{\mathrm{conv}}$
A (5.12)	$\mathrm{Pr}_0 K_{\mathrm{turb}} + \nu$	$\mathrm{Pr}_0 K_{\mathrm{turb}} + \nu$	$\mathrm{Pr}_0 K_{\mathrm{turb}} + \nu$	$\mathrm{Pr}_0 K_{\mathrm{conv}}$

ventional intrusions is illustrated in Fig. 13. For staircases, convection sets in at some critical intrusion amplitude and rapidly grows in extent (Fig. 13a). This is exactly the scenario suggested by Fig. 6. Conventional intrusions first develop stable layers, which rapidly give way to layers of diffusive convection and convection (Fig. 13b). Such behavior was also found by WR98, and prior to the onset of convection it matches the "I" scenario of Fig. 6.

From the numerical solutions, depth-averaged diapycnal and isopycnal fluxes of T and S can be calculated. (These are defined with respect to mean isopycnals, which here are level.) Results are expressed in terms of effective diffusion coefficients, defined as (mean flux)/

Fig. 11. Schematic illustration of coordinate system (χ, ζ), tilted with respect to (x, z) by an angle $-\theta = \tan^{-1}s$, where $s > 0$ is the intrusion slope. Also shown is the manner in which warm, salty intrusions rise across isopycnals (which here are horizontal), and cool, fresh intrusions sink.

(mean gradient). Three types of coefficients are considered: diapycnal coefficients $\mathcal{K}_T^{\mathrm{dif}}$ and $\mathcal{K}_S^{\mathrm{dif}}$ describing mixing by fingering, diffusive convection, and convection; diapycnal coefficients $\mathcal{K}_T^{\mathrm{adv}}$ and $\mathcal{K}_S^{\mathrm{adv}}$ describing diapycnal advection by intrusions; and isopycnal coefficients $\mathcal{K}_T^{\mathrm{iso}}$ and $\mathcal{K}_S^{\mathrm{iso}}$ describing isopycnal advection by intrusions. Results for the model runs in Fig. 12 and others are summarized in Table 3, where dimensional values are assigned based on estimated C-SALT conditions (Table 2). The diapycnal coefficients are independent of Γ_S, whereas the isopycnal coefficients scale as Γ_S^{-2} (see appendix).

Several key aspects of these results are now noted.

1) Mixing coefficients $\mathcal{K}_T^{\mathrm{dif}}$ and $\mathcal{K}_S^{\mathrm{dif}}$ are larger than coefficients K_T and K_S describing mixing by spatially uniform salt fingering. For the staircase run in Fig. 12, for example, $\mathcal{K}_T^{\mathrm{dif}} = 0.359$ cm^2 s^{-1} and $\mathcal{K}_S^{\mathrm{dif}} = 0.793$ cm^2 s^{-1}, whereas $K_T = 0.091$ cm^2 s^{-1} and $K_S = 0.212$ cm^2 s^{-1}.

2) The advective diapycnal fluxes are upgradient.

3) Total diapycnal heat fluxes, proportional to $\mathcal{K}_T^{\mathrm{dif}} + \mathcal{K}_T^{\mathrm{adv}}$, are sometimes upgradient for conventional intrusions, though not for staircases. Upgradient vertical fluxes of heat also were found in the analytical intrusion model of Garrett (1982). Total diapycnal salt fluxes are consistently downgradient.

4) Isopycnal mixing coefficients $\mathcal{K}_T^{\mathrm{iso}}$ and $\mathcal{K}_S^{\mathrm{iso}}$ are one to two orders of magnitude smaller for staircases than for conventional intrusions, perhaps because along-intrusion velocity is concentrated in the fingering interfaces.

It is evident from these results and from Fig. 9 that all of the numerical solutions of WR98 equilibrated as conventional intrusions because they considered $R_\rho = 1.6$ and Pr given by (5.11), choices for which staircases are excluded regardless of flux law and K_{turb}.

Finally, it was found that higher resolution was required for staircases than for conventional intrusions. Table 4 shows $\mathcal{K}_T^{\mathrm{dif}}$ and $\mathcal{K}_S^{\mathrm{dif}}$ versus resolution for the
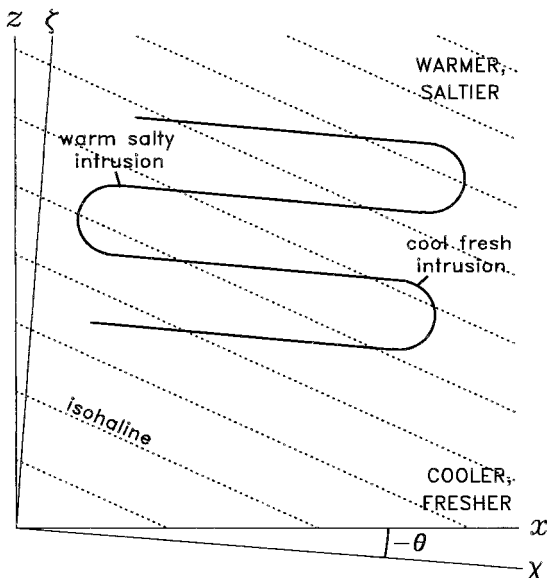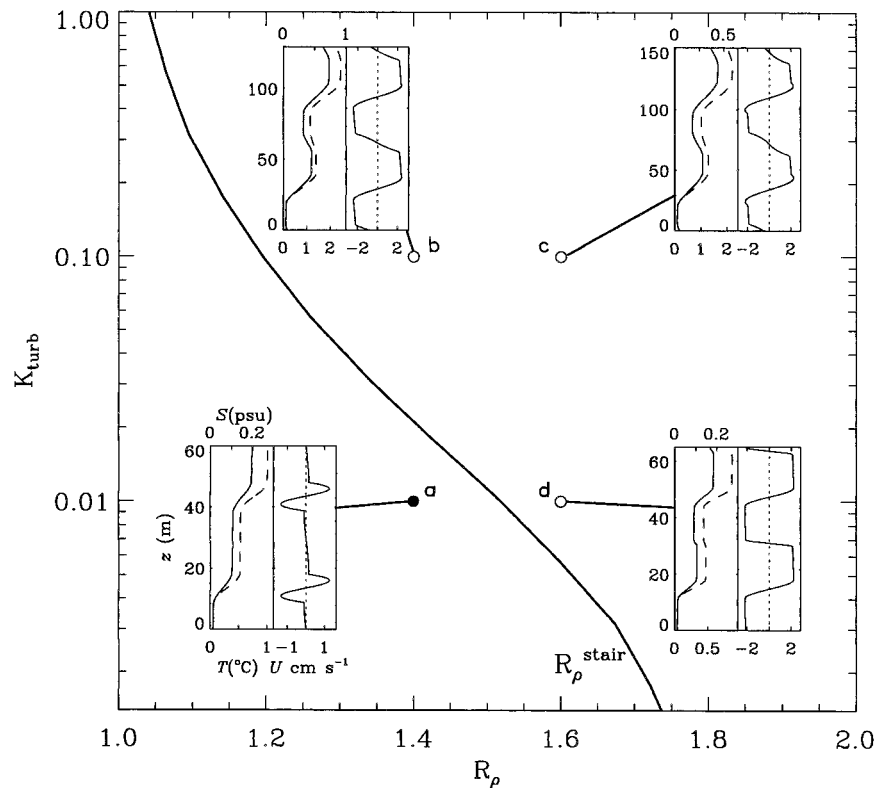
FIG. 12. Equilibria of intrusions under C-SALT conditions with flux law MG, Pr given by (5.12) with $Pr_0 = 1$, and R_ρ and K_{turb} as indicated. The heavy solid curve represents R_ρ^{stair}. Insets show profiles of S (solid curves in the left panels), T (dashed curves), and horizontal velocity u for equilibrated intrusions as functions of z. Conventional intrusions (open circles) are found where $R_\rho > R_\rho^{stair}$, whereas staircases (filled circle) are found where $R_\rho < R_\rho^{stair}$. For clarity, two repetitions of the periodic numerical solutions are shown.

$R_\rho = 1.4$ runs in Fig. 12. For the staircase run ($K_{turb} = 0.1$ cm^2 s^{-1}), the coefficients appear just to be converging when 512 Fourier modes are employed. However, the conventional intrusion run ($K_{turb} = 0.1$ cm^2 s^{-1}) appears nearly converged when just 64 Fourier modes are employed.

d. Comparison with observations

1) THRESHOLD R_ρ

An oft-noted property of oceanic staircases is that they appear only in locations having particularly low values of R_ρ. For example, the steps in the Western Mediterranean are characterized by $R_\rho \approx 1.1$–1.2 (Schmitt 1981; Krahmann 1997) and those beneath the Mediterranean outflow by $R_\rho \approx 1.3$. In the northwestern tropical Atlantic, the locale of the C-SALT experiment,

steps are confined to regions where $R_\rho \lesssim 1.7$ (Schmitt et al. 1987). There are no known instances of staircases having $R_\rho \gtrsim 1.7$.

The existence of staircases only in regions of sufficiently low R_ρ is in accord with the results in sections 6b,c. The threshold R_ρ^{stair} predicted from linear theory ranges from about 1.1 to more than 2, depending on turbulence levels and assumed laws for salt flux and viscous stress (Fig. 9). For R_ρ^{stair} to approach the observed threshold of 1.7, it is necessary to assume that turbulent mixing is extremely small ($K_{turb} \lesssim 0.01$ cm^2 s^{-1}), and that salt fingering does not contribute to viscous stress, that is, effective Prandtl number is given by (5.12).

The threshold R_ρ^{stair} also becomes larger when Pr_0 characterizing the ratio of effective viscosity to salt diffusivity is smaller than the value 10 used by WR98. For $Pr_0 = 1$ and fingering flux law MG, arguably the most

TABLE 2. Approximate conditions in C-SALT and Western Mediterranean staircases.

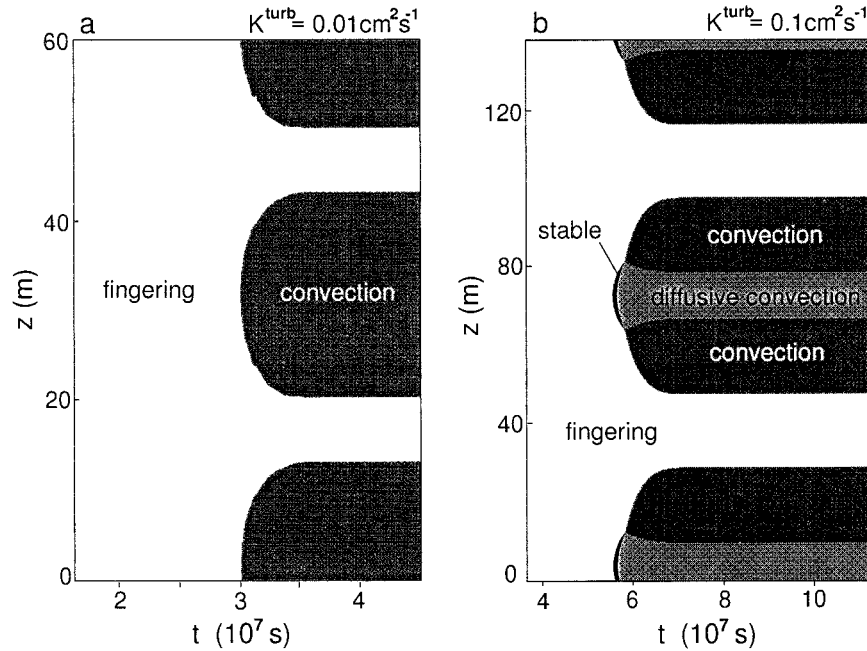| Staircase	R_ρ	Γ_S	N (s^{-1})	α (°C^{-1})	β (psu^{-1})
C-SALT	1.6	5×10^{-4}	3×10^{-3}	1.6×10^{-4}	7.8×10^{-4}
W. Mediterranean	1.1	1.3×10^{-3}	4×10^{-4}	2.2×10^{-4}	7.7×10^{-4}

FIG. 13. Evolution of intrusion structure for the $R_\rho = 1.4$ cases shown in Fig. 12, and conditions otherwise as in the C-SALT region (see Table 1): (a) $K_{turb} = 0.01$ cm^2 s^{-1}, intrusions evolve into staircase consisting of alternating fingering and convective layers; (b) $K_{turb} = 0.1$ cm^2 s^{-1}, equilibration is as conventional intrusions featuring a cyclical arrangement of fingering, convective, and diffusive convective layers. As in Fig. 12, the MG flux law is employed and Pr is given by (5.12) with $Pr_0 = 1$. Two repetitions of the periodic solutions are shown.

plausible because it is based on numerical simulations, R_ρ^{stair} reaches 1.52 when $K_{turb} = 0.01$ cm^2 s^{-1} and 1.76 when $K_{turb} = 0.001$ cm^2 s^{-1}.

2) HEIGHT OF STEPS

According to the theory in this section, thermohaline step height (mixed layer plus interface) can be identified with intrusion wavelength. To evaluate the latter requires a knowledge of N, R_ρ, and Γ_S. For at least two staircases, these quantities can be estimated from published data, as summarized in Table 2. Evaluation of wavelength also requires specification of fingering and

turbulent fluxes, and as throughout this section a range of choices is considered.

The mean step height in the core of the western tropical North Atlantic (C-SALT) staircase appears to be 30 or 40 m (Schmitt et al. 1987), as indicated by the vertical dashed lines in Figs. 14a,b. Predicted step heights tend to exceed the observed values, but fall within the observed range for flux law MG when Pr is specified by (5.12) with $Pr_0 < 10$, and turbulence is weak ($K_{turb} \lesssim 0.02$ cm^2 s^{-1}).

In the Algerian and Provencal Basins of the western Mediterranean, observed step heights are typically 60 to 100 m (Krahmann 1997). In this case (Figs. 14c,d),

TABLE 3. Effective diffusion coefficients (in cm^{2}s^{-1}) for equilibrated model runs, assuming $\Gamma_S = 5 \times 10^{-4}$. Superscript "dif" applies to diapycnal diffusive mixing, "adv" to diapycnal advective mixing, and "iso" to isopycnal advective mixing. The first four runs correspond to those shown in Fig. 12. Resolution: 512 Fourier modes for staircases, and 128 Fourier modes for conventional intrusions.

R_ρ	K_{turb}	Flux law	Pr	Pr_0	$\mathcal{K}^{dif}_T$	$\mathcal{K}^{dif}_S$	$\mathcal{K}^{adv}_T$	$\mathcal{K}^{adv}_S$	$\mathcal{K}^{iso}_T$	$\mathcal{K}^{iso}_S$	Config*
1.4	0.01	MG	5.12	1	0.359	0.793	−0.013	−0.011	3.32×10^5	2.07×10^5	S
1.4	0.1	MG	5.12	1	0.306	0.789	−0.305	−0.401	1.03×10^7	0.97×10^7	I
1.6	0.01	MG	5.12	1	0.148	0.566	−0.137	−0.162	0.51×10^7	0.38×10^7	I
1.6	0.1	MG	5.12	1	0.256	0.726	−0.226	−0.340	1.21×10^7	1.13×10^7	I
1.4	0.01	WR2	5.12	10	0.567	1.23	−0.040	−0.033	1.04×10^6	6.10×10^5	S
1.4	0.1	WR2	5.12	10	0.647	2.28	−1.05	−1.35	3.59×10^7	3.30×10^7	I
1.4	0.01	WR2	5.11	10	0.299	3.41	−1.91	−2.17	6.88×10^7	5.59×10^7	I
1.4	0.1	WR2	5.11	10	0.458	2.26	−1.16	−1.44	4.73×10^7	4.21×10^7	I
1.6	0.1	WR2	5.11	10	0.429	1.77	−0.538	−0.753	3.23×10^7	3.82×10^7	I
1.6	0.1	WR0	5.11	10	0.568	3.24	−0.974	−1.29	5.61×10^7	4.64×10^7	I

* S: staircase; I: conventional intrusion.

TABLE 4. Dependence of effective diffusion coefficients on resolution for $R_p = 1.4$ runs shown in Fig. 12 (units of cm²s⁻¹).

Fourier modes	Staircases		Convective intrusions	
	$\mathcal{K}^{\text{dif}_T}$	$\mathcal{K}^{\text{dif}_S}$	$\mathcal{K}^{\text{dif}_T}$	$\mathcal{K}^{\text{dif}_S}$
64	0.353	0.779	0.297	0.770
128	0.359	0.793	0.306	0.789
256	0.277	0.619	0.301	0.777
512	0.264	0.573	0.303	0.754

predicted step heights fall within the observed range for all flux laws provided Pr is specified by (5.12), and $K_{\text{turb}} \lesssim 0.05$ cm² s⁻¹ (Pr₀ = 10) or 0.05 cm² s⁻¹ $\lesssim K_{\text{turb}} \lesssim$ 0.2 cm² s⁻¹ (case MG; Pr₀ = 1).

3) LATERAL PROPERTY VARIATIONS

When followed laterally, staircase layers are found to lie across isopycnals, and to become warmer and saltier as their density increases. Such a trend, documented for the C-SALT staircase by Schmitt et al. (1987) and for the western Mediterranean by Zodiatis and Gasparini (1996) and Krahmann (1997), is identical to that ex-

hibited by salt finger-driven intrusions (WR95): cool and fresh intrusions sink across isopycnals, becoming warmer and saltier as they mix diffusively with warmer, saltier intrusions above and below (Fig. 11).

4) LATERAL DENSITY RATIO

In the C-SALT staircase, lateral variations of layer temperature and salinity are related by $\alpha T_\chi/\beta S_\chi = 0.85 \pm 0.03$ (Schmitt 1994). In the western Mediterranean, this ratio is 0.9 ± 0.06 (Krahmann 1997).

For intrusions driven by uniform background gradients, lateral density ratio depends on the gradients and intrusion slope, and is given by

$$\frac{\alpha T_\chi}{\beta S_\chi} = \frac{\alpha}{\beta} \frac{\cos\theta \overline{T}_x + \sin\theta \overline{T}_z}{\cos\theta \overline{S}_x + \sin\theta \overline{S}_z} = \frac{\Gamma_S - s\overline{R}_\rho}{\Gamma_S - s}. \quad (5.23)$$

Figure 15 compares the observed lateral density ratios with (5.23) evaluated for the fastest-growing mode. For the C-SALT staircase, predicted ratios lie within the error bars for all three flux laws provided that Pr is given by (5.12), and $K_{\text{turb}} \lesssim 0.01$ cm² s⁻¹ (Figs. 15a,b). (For case MG, Pr₀ $\lesssim 2$ is required as well.) For the
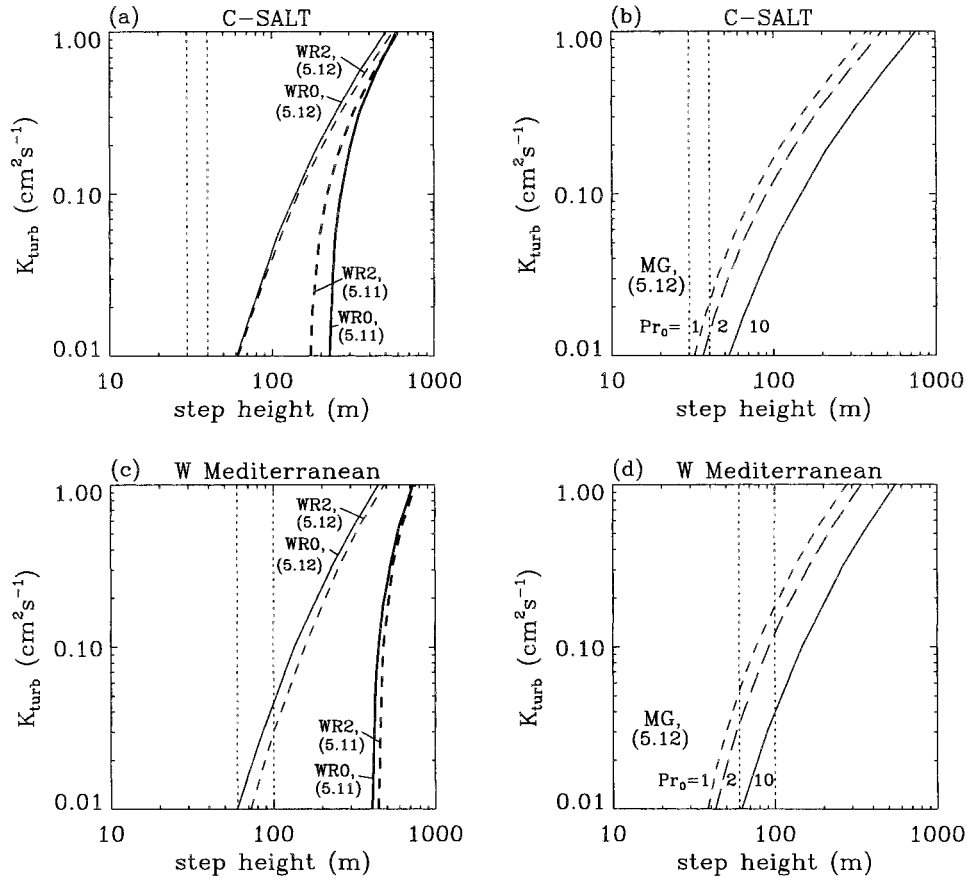

FIG. 14. Predicted vs observed step heights for the C-SALT (a,b) and Western Mediterranean (c,d) staircases. The curves denote predicted step heights for the choices of flux law and Pr considered in Fig. 9. Dotted vertical lines indicate ranges of observed step heights.
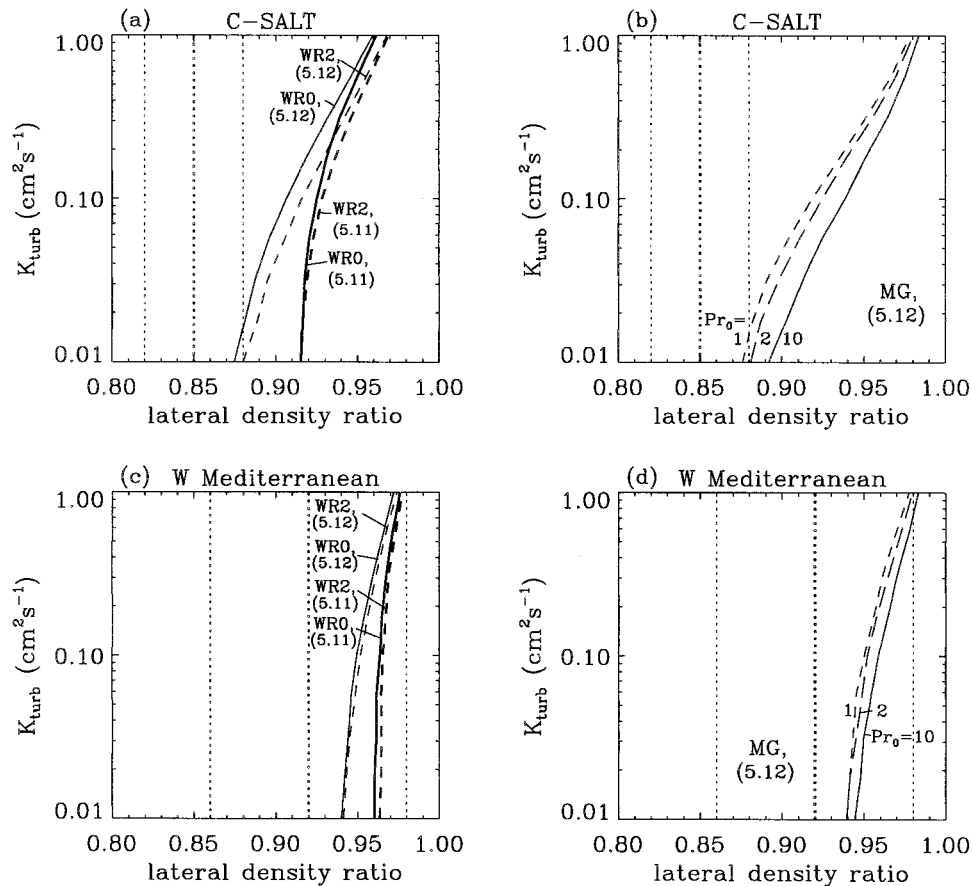
FIG. 15. Predicted vs observed lateral density ratios $\alpha T_\chi/\beta S_\chi$ for the C-SALT (a,b) and Western Mediterranean (c,d) staircases. The curves denote predicted ratios for the choices of flux law and Pr considered in Fig. 9. Heavy dotted lines denote observed values and light dotted lines the uncertainties, as reported by Schmitt (1994) and Krahmann (1997).

Western Mediterranean staircase, predicted ratios lie within the error bars under all conditions shown, although optimal agreement with the centroid value 0.92 again is realized when K_{turb} is small and Pr is given by (5.12) with $Pr_0 < 10$ (Figs. 15c,d).

Other proposed explanations for the observed lateral density ratios include modification of water properties by combined effects of salt fingering and turbulence (Marmorino 1990; Schmitt 1994), and interfacial advection due to nonlinearities in the equation of state (McDougall 1991).

5) LAYER SLOPES

As mentioned above, staircase mixed layers slope across isopycnals in the same sense as intrusions. Slopes were estimated for the C-SALT and Mediterranean steps using

$$\rho_\chi = \sin\theta \overline{\rho}_z \approx -s\overline{\rho}_z. \qquad (5.24)$$

The lateral density gradient ρ_χ was estimated from Fig. 5 of Schmitt et al. (1987) and Fig. 4 of Krahmann (1997)

by dividing total lateral density contrast within a given layer by the approximate horizontal extent of the staircase. These estimates are somewhat uncertain because they assume that ρ_χ is uniform.

For the C-SALT staircase, estimated slope exceeds the theoretical slopes (Figs. 16a,b). However, the disagreement is least ($\lesssim 20\%$) for $K_{turb} \lesssim 0.01$ cm^2 s^{-1} and Pr law (5.12) with $Pr_0 < 10$. For the Western Mediterranean staircase, estimated slope again exceeds the theoretical slopes (Figs. 16c,d). Disagreement is again minimized by $K_{turb} \lesssim 0.01$ cm^2 s^{-1} and Pr law (5.12) with $Pr_0 < 10$, although this time the remaining discrepancy is approximately a factor of 3.

6) SHEAR IN FINGERING INTERFACES

The numerical solutions described above indicate that, for staircases, intrusion shear is highly concentrated in the fingering interface. In the staircase illustrated in Fig. 12a, shear attains 0.8×10^{-2} s^{-1} in the center of the fingering interface (Fig. 17a), and gradient Rich-
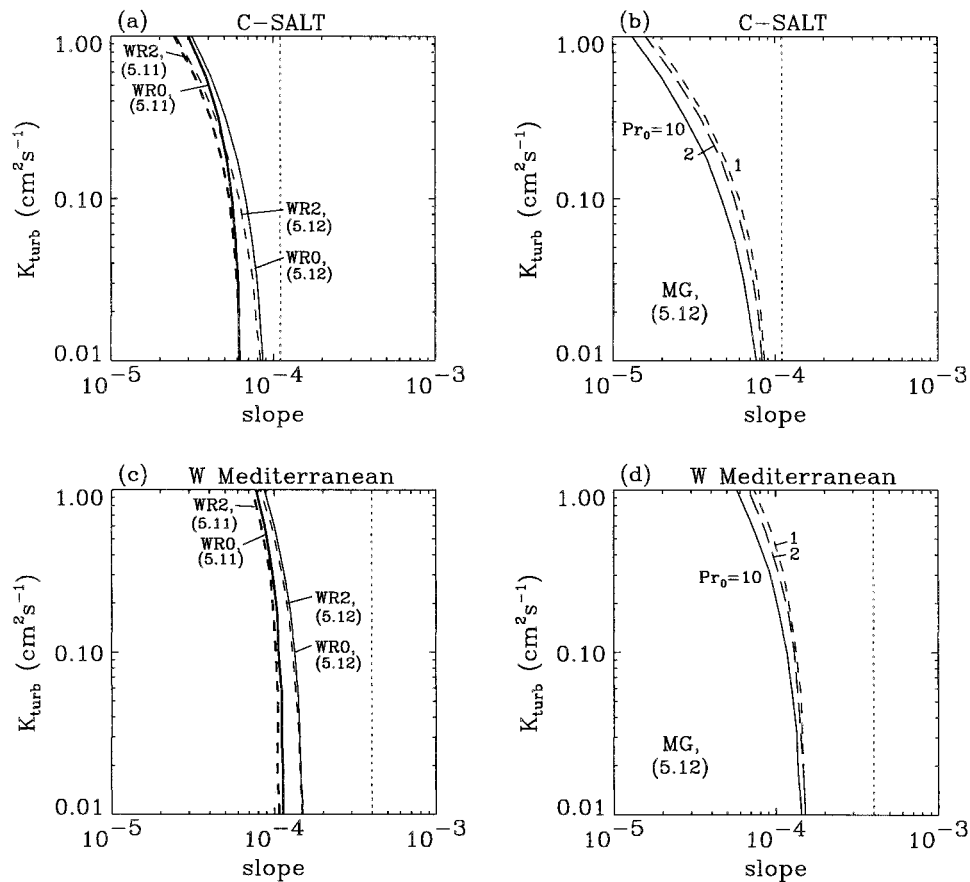
FIG. 16. Predicted vs observed cross-isopycnal slope for the C-SALT (a,b) and Western Mediterranean (c,d) staircases. The curves indicate predicted ratios for the choices of flux law and Pr considered in Fig. 9. Dotted vertical lines denote estimated cross-isopycnal slopes from data of Schmitt (1994) and Krahmann (1997).

ardson number $Ri = N^2/u_z^2$ reaches a minimum of 0.9 (Fig. 17d).

Observations indicate that shear indeed is concentrated in fingering interfaces. In the C-SALT staircase ($R_\rho \lesssim 1.6$), interface shears averaged over 0.5-m intervals sometimes exceed 10^{-2} s^{-1} (Gregg and Sanford 1987; Gregg 1988). While such values are in accord with Fig. 17a, the double-jet structure seen in Fig. 12a is not obviously present in the observed horizontal velocities. However, other sources of shear are present which could mask such signals in an instantaneous profile. Richardson numbers computed from average gradients across interfaces range between 1 and 5.

Shears in the staircase beneath the Mediterranean outflow ($R_\rho \approx 1.3$) were examined by Simpson et al. (1979). Shears evaluated from differences over 1 m again were highest in the interfaces. Interface shear profiles typically were multipronged as in Fig. 17b, although interpretation as a signature of double jets is tempered by the relatively low resolution and the presence of layered substructure in some of the interfaces. In profiles of velocity there is some suggestion of ~1 cm s^{-1} inter-

facial jets oriented NE–SW, but too little data is shown for a definitive assessment. Interfacial gradient Richardson numbers were between 0.3 and 1, with uncertainties of up to 30%.

Shear measurements also were taken by Evans (1981) for a rather weak staircase embedded in a Mediterranean salt lens north of Haiti ($R_\rho \approx 1.5$ to 1.7). Shear computed on 2-m intervals is again much higher in interfaces than in layers, although shears within the staircase are much smaller than in waters above and below.

7) COEXISTENCE OF STEPS AND INTRUSIONS

In thermohaline staircases, prominent T and S inversions that resemble conventional intrusions can appear in place of steps. Such features sometimes replace individual steps near the top of an otherwise normal staircase. This is seen in the C-SALT region (Mazeika 1974, Fig. 2; Marmorino et al. 1987, Fig. 6), beneath the Mediterranean outflow (Tait and Howe 1968, Fig. 2; Tait and Howe 1971, Fig. 2), and in the Tyrrhenian Sea (Zodiatis and Gasparini 1996, Fig. 5). Observations
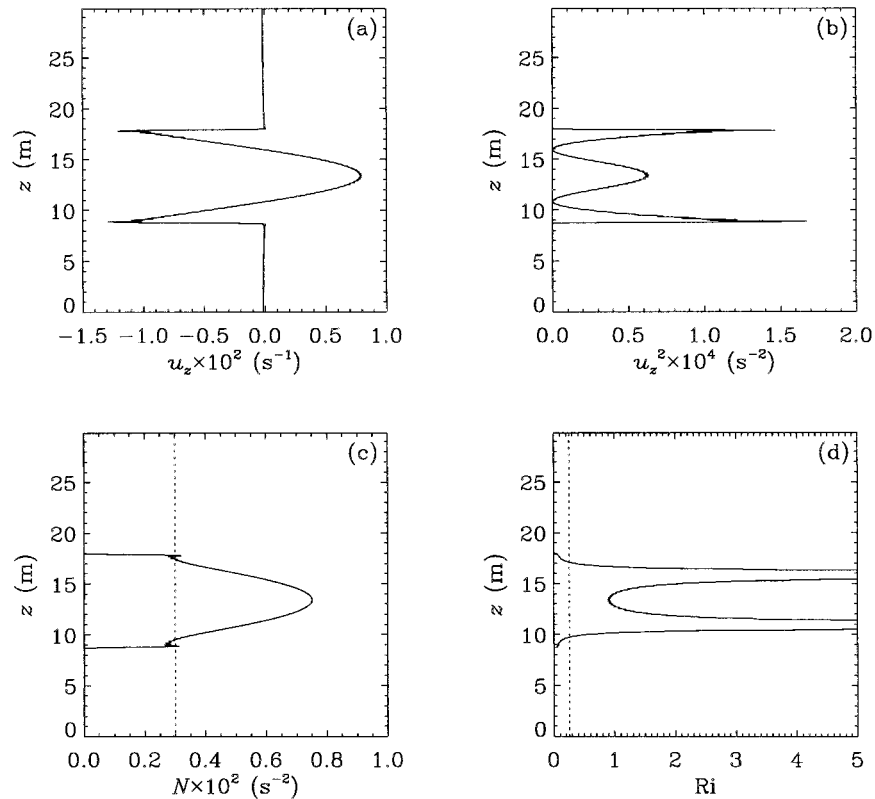
FIG. 17. For a staircase step depicted in Fig. 12a, vertical profiles of (a) shear u_z; (b) shear squared; (c) buoyancy frequency N (dotted line indicates background value); (d) gradient Richardson number (dotted line indicates critical value 0.25). Except for $R_\rho = 1.4$, C-SALT conditions are assumed (Table 2).

show that R_ρ tends to increase upward near the tops of staircases (e.g., Schmitt 1994). The appearance of inversions instead of steps thus may result from R_ρ locally exceeding R_ρ^{stair}. This conjecture is supported by data of Zodiatis and Gasparini (1996), who show two temperature profiles taken 5 months apart. In the later profile, the uppermost large step has become inverted, while R_ρ has increased from 1.26 to 1.6. (An inversion is also developing at the top of the second large step, for which R_ρ has increased from 1.19 to 1.25.)

Staircases also can evolve laterally into intrusions, especially in the presence of steepening horizontal gradients. In the C-SALT area, for example, staircases develop inversions near thermohaline fronts associated with eddies (Zhurbas et al. 1988; Marmorino 1991) and the staircase edge (Zhurbas and Ozmidov 1983; Marmorino et al. 1987). In the Western Mediterranean, such a transition occurs in the proximity of higher horizontal gradients where Levantine Intermediate Water enters the Algerian Basin (Krahmann 1997).

Assuming R_ρ is horizontally uniform, at least two possible reasons are evident for why staircases develop inversions near thermohaline fronts. The first, for which there is little evidence, is that turbulent mixing is systematically larger within such fronts. This would in-

crease R_ρ^{stair} (Fig. 9). If the elevated threshold exceeded ambient R_ρ, conventional intrusions instead of steps would develop within the front.

A second possibility is related to factors determining the vertical scale of intrusions near fronts. Suppose first that a region of low horizontal gradients contains fully developed steps and that a higher-gradient region develops adjacent to it, perhaps at the staircase edge or within an eddy. Such a situation is illustrated in Fig. 18a, where growth rates are contoured for low-gradient [$\Gamma_S = (\Gamma_S)_0$] and higher-gradient [$\Gamma_S = 2(\Gamma_S)_0$] regions. Plus signs denote where staircases are preferred, and minus signs where conventional intrusions are preferred. If the existing large-amplitude steps in the low-gradient region (left panel) induce growth at like wavenumber m in the higher-gradient region, the latter disturbances will develop as conventional intrusions (right panel, solid dot).

Conversely, it seems plausible that under some conditions intrusions established at a front will propagate away from the front without altering their vertical scale (Fig. 18b). In this case, if conventional intrusions are preferred in the high-gradient region (right panel), intrusions having like m in the low-gradient region will develop as staircases (left panel, solid dot). Both of these
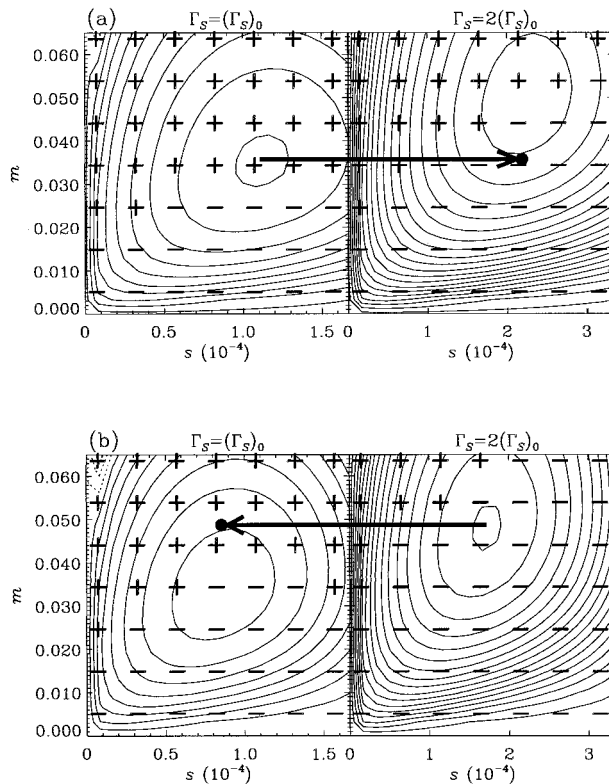
FIG. 18. Schematic illustration of two possible scenarios by which steps could evolve laterally into conventional intrusions near thermohaline fronts. Here the solid contours denote positive growth rates, and dashed contours negative growth rates. Plus signs indicate (m, s) where steps are favored on the basis of (5.10), and minuses where conventional intrusions are favored. (a) Step size set by low-gradient region. Suppose, for example, that an eddy leads to increased horizontal gradients (increased Γ_S). The existing steps in the low-gradient region (left) might lead to intrusions at like m in the high-gradient region (right; solid dot) even though growth rate is not maximized. In this example, the intrusions in the high-gradient region would develop as conventional intrusions. (b) Step size set by high-gradient region. Suppose that the low-gradient region initially does not contain intrusions, and that growing intrusions in the high-gradient region (right) retain their characteristic m as they propagate into the low-gradient region (left; solid dot). In this example, conventional intrusions in the high-gradient region would become steps in the low-gradient region.

scenarios replicate the observed tendency for conventional intrusions at a front to evolve into staircases away from the front.

e. Discussion

The theory for thermohaline staircases developed in this section appears able to account for a cutoff value for R_ρ, as well as observed staircase properties. Predictions and observations tend to be in closest agreement when salt fingers are assumed not to appreciably contribute to shear stress, when the turbulent Prandtl number is of order unity, and when turbulent mixing is very weak ($K_{\text{turb}} \lesssim 0.01$ cm^2 s^{-1}).

Such low turbulent mixing may not be implausible. In the C-SALT staircase, turbulence due to breaking internal waves is even weaker than the generally low levels found elsewhere in the thermocline (Schmitt 1994), which can be <0.1 cm^2 s^{-1} throughout large regions (e.g., Polzin et al. 1997). Marmorino (1990) concludes that turbulent mixing in this region increases buoyancy flux 10%–20% over that of fingers acting alone. The buoyancy mixing coefficient for fingering is

$$K_\rho^f = (K_S^f - R_\rho K_T^f)/(1 - R_\rho)$$

(Shen 1995). For $K_T^f = 0.063$ cm^2 s^{-1} and $K_S^f = 0.167$ cm^2 s^{-1} (flux law MG with $R_\rho = 1.6$), $K_\rho^f = -0.112$ cm^2 s^{-1}. Because $K_\rho = K_{\text{turb}}$ under the assumed turbulent flux law (equal mixing of T and S), Marmorino's estimate yields $K_{\text{turb}} = 0.01$–0.02 cm^2 s^{-1}. Turbulent mixing coefficients as low as 0.01 cm^2 s^{-1} have been found in the core of the Pacific Equatorial Undercurrent (Peters et al. 1988).

While the comparisons in section 5c are encouraging, it should be emphasized that they are based upon crude estimates of hydrographic parameters from published data. Estimates of Γ_S and layer slope are especially uncertain because they suppose uniform lateral gradients across the staircase region and ignore possible along-front contributions to slope. Gradients certainly are not uniform in the Western Mediterranean (Krahmann 1997, his Fig. 11), which may account for the relatively large discrepancy between observed and predicted slopes (Figs. 16c,d).

It should be emphasized that the above theory does not account for baroclinic effects and that their likely importance in the C-SALT region and Western Mediterranean has not been assessed. A stability theory for intrusions that accounts for baroclinic shear has been developed by May and Kelly (1997), and it should not be too difficult to extend the procedure described in section 5b to the baroclinic case.

Finally, the theory developed here does not explain at least one observed property of staircases, the presence of sublayering within fingering interfaces (Williams 1975; Marmorino 1989).

6. Summary and conclusions

This paper has sought to assess four hypotheses concerning the origin of thermohaline staircases. The hypothesis that staircases arise from double-diffusive intrusions was developed into a quantitative theory, consistent with a number of observed staircase properties. Using the stability theory of WR98, it was shown that intrusions can evolve toward staircase configurations if R_ρ and turbulent mixing coefficient K_{turb} are sufficiently small. This is in accord with observations showing that $R_\rho \lesssim 1.7$ and K_{turb} is unusually small in staircase regions.

In considering a range of parameter values and flux prescriptions, turbulent diffusivities $K_{\text{turb}} \lesssim 0.01$ cm^2 s^{-1} and effective viscosities (5.12) that include no con-

tribution from fingering tended to yield closest agreement with observations. Quantities then predicted with reasonable accuracy included step heights, lateral density ratios, layer slopes, and the threshold R_ρ^{stair}, although such comparisons were based on rough estimates of lateral gradients and slopes and could be improved.

Numerical solutions confirmed that staircases are viable equilibria of intrusions. The equilibrated solutions exhibit pronounced shears within the fingering interfaces (Fig. 12). These shears, coupled with the lateral gradients in T and S, provide a means for maintaining the large interfacial gradients, and might be observable.

The remaining hypotheses for staircase formation differ from the intrusion hypothesis in that they require only vertical gradients to operate. The collective instability hypothesis of Stern (1969) and the multiple equilibrium hypothesis are in accord with aspects of step formation observed in the laboratory, but remain to be linked convincingly to the fingering staircases observed in the oceans. The negative density diffusion hypothesis in its more realistic formulation (sec. 4b) resembles the multiple equilibrium hypothesis in that finite-amplitude disturbances are necessary to generate steps.

These one-dimensional mechanisms could be responsible for the observed tendency of staircase interfaces to form sublayers (Williams 1975; Linden 1978; Marmorino 1989), a phenomenon for which the intrusion hypothesis as formulated here offers no explanation.

Although the intrusion hypothesis for staircases appears promising, more accurate and detailed observational comparisons should be undertaken. Further work is also needed to improve prescriptions for fluxes and to incorporate baroclinic effects, which have been neglected here. Finally, it would be worthwhile to explore the applicability of the intrusion hypothesis to staircases in regions of diffusive convection.

APPENDIX

Similarity Relations for Intrusions

It is shown here that when slope is small, solutions to intrusion evolution equations (5.18)–(5.20) obey simple scaling relations with respect to changes in isohaline tilt $\Gamma_S = \overline{S}_x/\overline{S}_z$. In the limit $s \ll 1$, (5.18)–(5.20) become

$$Z_t = -\theta(T - S)_\zeta + (AZ)_{\zeta\zeta}, \tag{A.1}$$

$$T_t = -U(\overline{T}_x + \theta\overline{T}_z) + (K_T T_\zeta)_\zeta, \tag{A.2}$$

$$S_t = -U(\overline{S}_x + \theta\overline{S}_z) + (K_S S_\zeta)_\zeta, \tag{A.3}$$

to $O(\theta^2)$. Consider the transformation

$$t \to C^{-1}t, \tag{A.4}$$

$$\zeta \to C^{-1/2}\zeta, \tag{A.5}$$

$$\theta \to C\theta, \tag{A.6}$$

$$\overline{T}_x \to C\overline{T}_x, \tag{A.7}$$

$$\overline{S}_x \to C\overline{S}_x, \tag{A.8}$$

$$\overline{T}_z \to \overline{T}_z, \tag{A.9}$$

$$\overline{S}_z \to \overline{S}_z, \tag{A.10}$$

$$T \to C^{-1/2}T, \tag{A.11}$$

$$S \to C^{-1/2}S, \tag{A.12}$$

$$U \to C^{-1/2}U, \tag{A.13}$$

$$Z \to Z, \tag{A.14}$$

which implies $\Gamma_S \to C\Gamma_S$, and to which (A.1)–(A.3) are invariant. Intrusion growth rate, slope, and wavenumber thus obey

$$\lambda \propto \Gamma_S, \tag{A.15}$$

$$\theta \propto \Gamma_S, \tag{A.16}$$

$$m \propto \Gamma_S^{1/2}. \tag{A.17}$$

Similarly, the isopycnal flux $\mathcal{F}_T^{\text{iso}}$ and mixing coefficient $\mathcal{K}_T^{\text{iso}}$ for heat obey

$$\mathcal{F}_T^{\text{iso}} = \overline{U\cos\theta T} \propto \Gamma_S^{-1}, \tag{A.18}$$

$$\mathcal{K}_T^{\text{iso}} = \mathcal{F}_T^{\text{iso}}/\overline{T}_x \propto \Gamma_S^{-2}; \tag{A.19}$$

likewise for salinity. By contrast, the diapycnal fluxes and mixing coefficients are independent of Γ_S:

$$\mathcal{F}_T^{\text{adv}} = \overline{U\sin\theta T}, \tag{A.20}$$

$$\mathcal{F}_T^{\text{dif}} = \overline{K_T T_\zeta \cos\theta}, \tag{A.21}$$

$$\mathcal{K}_T^{\text{adv}} = \mathcal{F}_T^{\text{adv}}/\overline{T}_z, \tag{A.22}$$

$$\mathcal{K}_T^{\text{dif}} = \mathcal{F}_T^{\text{dif}}/\overline{T}_z \tag{A.23}$$

(likewise for S), where "adv" denotes the effect of along-intrusion advection, and "dif" the effect of small-scale vertical mixing.

REFERENCES

Boyd, J. D., 1989: Properties of thermal staircases off the northeast coast of South America, spring and fall 1985. *J. Geophys. Res.,* **94,** 8303–8312.

——, and H. Perkins, 1987: Characteristics of thermohaline steps off the northeast coast of South America, July 1983. *Deep-Sea Res.,* **34,** 337–364.

Canuto, C., M. Y. Hussaini, A. Quarteroni, and T. A. Zang, 1988: *Spectral Methods in Fluid Mechanics.* Springer, 567 pp.

Cooper, J. W., and H. Stommel, 1968: Regularly spaced steps in the main thermocline near Bermuda. *J. Geophys. Res.,* **73,** 5849–5854.

Elliott, A. J., and R. I. Tait, 1977: The nature of the Mediterranean outflow step structure. *A Voyage of Discovery, G. Deacon 70th Anniversary Volume, Deep-Sea Res.* (Suppl.), 213–220.

——, M. R. Howe, and R. I. Tait, 1974: The lateral coherence of a system of thermo-haline layers in the deep ocean. *Deep-Sea Res.,* **21,** 95–107.

Evans, D. L., 1981: Velocity shear in a thermohaline staircase. *Deep-Sea Res.,* **28A,** 1409–1415.

Fleury, M., and R. G. Lueck, 1991: Fluxes across a thermohaline interface. *Deep-Sea Res.,* **38,** 745–769.

Garrett, C., 1982: On the parameterization of diapycnal fluxes due to double-diffusive intrusions. *J. Phys. Oceanogr.,* **12,** 952–959.

Gregg, M. C., 1975: Microstructure and intrusions in the California Current. *J. Phys. Oceanogr.,* **5,** 253–278.

——, 1988: Mixing in the thermohaline staircase east of Barbados. *Small-Scale Turbulence and Mixing in the Ocean,* J. C. J. Nihoul and B. M. Jamart, Eds., Elsevier, 453–470.

——, and T. B. Sanford, 1987: Shear and turbulence in thermohaline staircases. *Deep-Sea Res.,* **34,** 1689–1696.

Griffiths, R. W., and B. R. Ruddick, 1980: Accurate fluxes across a salt–sugar interface deduced from direct density measurements. *J. Fluid Mech.,* **99,** 85–95.

Holyer, J. Y., 1981: On the collective instability of salt fingers. *J. Fluid Mech.,* **110,** 195–207.

——, 1984: The stability of long, steady, two-dimensional salt fingers. *J. Fluid Mech.,* **147,** 169–185.

——, 1985: The stability of long steady three-dimensional salt fingers to long-wavelength perturbations. *J. Fluid Mech.,* **156,** 495–503.

Horne, E. P. W., 1978: Interleaving at the subsurface front in the slope water off Nova Scotia. *J. Geophys. Res.,* **83,** 3659–3671.

Howard, L. N., and G. Veronis, 1992: Stability of salt fingers with negligible diffusivity. *J. Fluid Mech.,* **239,** 511–522.

Howe, M. R., and R. I. Tait, 1970: Further observations of thermohaline stratification in the deep ocean. *Deep-Sea Res.,* **17,** 963–972.

Johannessen, O. M., and O. S. Lee, 1974: A deep stepped thermohaline structure in the Mediterranean. *Deep-Sea Res.,* **21,** 629–639.

Kelley, D., 1984: Effective diffusivities within oceanic thermohaline staircases. *J. Geophys. Res.,* **89,** 10 484–10 488.

Kerr, O. S., and J. Y. Holyer, 1986: The effect of rotation on double-diffusive interleaving. *J. Fluid Mech.,* **162,** 23–33.

Krahmann, G., 1997: Horizontal variability of thermohaline staircases in the western Mediterranean. *Double-Diffusive Processes, 1996 Summer Study Program in Geophysical Fluid Dynamics,* S. Meacham and D. Tucholke, Eds., Woods Hole Oceanogr. Inst. Tech. Rep. WHOI-97-10, 331–347.

Kunze, E., 1987: Limits on growing, finite-length salt fingers: A Richardson number constraint. *J. Mar. Res,* **45,** 533–556.

——, 1995: Quantifying salt-fingering fluxes in the ocean. *Double-Diffusive Convection, Geophys. Monogr.,* No. 94, Amer. Geophys. Union, 313–320.

——, A. J. Williams III, and R. W. Schmitt, 1987: Optical microstructure in the thermohaline staircase east of Barbados. *Deep-Sea Res.,* **34,** 1697–1704.

Kuzmina, N. P., and V. B. Rodionov, 1992: Influence of baroclinicity on formation of thermohaline intrusions in ocean frontal zones (English translation). *Izv. Atmos. Oceanogr. Phys.,* **28,** 804–810.

Lambert, R. B., and J. W. Demenkow, 1971: On the vertical transport due to fingers in double-diffusive convection. *J. Fluid Mech.,* **54,** 627–640.

——, and W. Sturges, 1977: A thermohaline staircase and vertical mixing in the thermocline. *Deep-Sea Res.,* **24,** 211–222.

Linden, P. F., 1973: On the structure of salt fingers. *Deep-Sea Res.,* **20,** 325–340.

——, 1976: The formation and destruction of fine-structure by double-diffusive processes. *Deep-Sea Res.,* **23,** 895–908.

——, 1978: The formation of banded salt finger structure. *J. Geophys. Res.,* **83,** 2902–2912.

Lueck, R. G., 1987: Microstructure measurements in a thermohaline staircase. *Deep-Sea Res.,* **34,** 1677–1688.

Magnell, B., 1976: Salt fingers observed in the Mediterranean outflow region (34°N, 11°W) using a towed sensor. *J. Phys. Oceanogr.,* **6,** 511–523.

Marmorino, G. O., 1989: Substructure of oceanic salt finger interfaces. *J. Geophys. Res.,* **94,** 4891–4904.

——, 1990: ''Turbulent mixing'' in a salt finger staircase. *J. Geophys. Res.,* **95,** 12 983–12 994.

——, 1991: Intrusions and diffusive interfaces in a salt-finger staircase. *Deep-Sea Res.,* **38,** 1431–1454.

——, W. K. Brown, and W. D. Morris, 1987: Two-dimensional temperature structure in the C-SALT thermohaline staircase. *Deep-Sea Res.,* **34,** 1667–1676.

May, B. D., and D. E. Kelly, 1997: Effect of baroclinicity on double-diffusive interleaving. *J. Phys. Oceanogr.,* **27,** 1997–2008.

Mazeika, P. A., 1974: Subsurface mixed layers in the northwestern tropical Atlantic. *J. Phys. Oceanogr.,* **4,** 446–453.

McDougall, T. J., 1985: Double-diffusive interleaving. Part I: Linear stability analysis. *J. Phys. Oceanogr.,* **11,** 1523–1541.

——, 1991: Interfacial advection in the thermohaline staircase east of Barbados. *Deep-Sea Res.,* **38,** 357–370.

——, and J. R. Taylor, 1984: Flux measurements across a finger interface at low values of the stability ratio. *J. Mar. Res.,* **42,** 1–14.

Miller, R. R., and D. G. Browning, 1974: Thermal layering between the Galápagos Islands and South America. *Deep-Sea Res.,* **21,** 669–673.

Molcard, R., and R. I. Tait, 1977: The steady state of the step structure in the Tyrrhenian Sea. *A Voyage of Discovery, George Deacon 70th Anniversary Volume, Deep-Sea Res.* (Suppl.), 221–233.

Muench, R. D., H. J. S. Fernando, and G. R. Stegun, 1990: Temperature and salinity staircases in the northwestern Weddell Sea. *J. Phys. Oceanogr.,* **20,** 295–306.

Neshyba, S., V. T. Neal, and W. Denner, 1971: Temperature and conductivity measurements under ice-island T-3. *J. Geophys. Res.,* **76,** 8107–8120.

Niino, H., 1986: A linear stability theory of double-diffusive horizontal intrusions in a temperature-salinity front. *J. Fluid Mech.,* **171,** 71–100.

Özgökmen, T. M., O. E. Esenkov, and D. B. Olson, 1998: A numerical study of layer formation due to fingers in double-diffusive convection. *J. Mar. Res.,* **56,** 463–487.

Padman, L., and T. M. Dillon, 1987: Vertical fluxes through the Beaufort Sea thermohaline staircase. *J. Geophys. Res.,* **92,** 10 799–10 806.

Peters, H., M. C. Gregg, and J. M. Toole, 1988: On the parameterization of equatorial turbulence. *J. Geophys. Res.,* **93,** 1199–1218.

Polzin, K. L., J. M. Toole, J. R. Ledwell, and R. W. Schmitt, 1997: Spatial variability of turbulent mixing in the abyssal ocean. *Science,* **276,** 93–96.

Ruddick, B., 1985: Momentum transport in thermohaline staircases. *J. Geophys. Res.,* **90,** 895–902.

——, 1992: Intrusive mixing in a Mediterranean salt lens–intrusion slopes and dynamical mechanisms. *J. Phys. Oceanogr.,* **22,** 1274–1285.

——, R. W. Griffiths, and G. Symonds, 1989: Frictional stress across a sheared double-diffusive interface. *J. Geophys. Res.,* **94,** 18 161–18 173.

Rudels, B., G. Björk, R. D. Muench, and U. Schauer, 1999: Double-diffusive layering in the Eurasian Basin of the Arctic Ocean. *J. Mar. Syst.,* **21,** 3–27.

Schmitt, R. W., 1979: Flux measurements on salt fingers at an interface. *J. Mar. Res.,* **37,** 419–436.

——, 1981: Form of the temperature–salinity relationship in the Cen-

tral Water: Evidence for double-diffusive mixing. *J. Phys. Oceanogr.,* **11,** 1015–1026.

——, 1988: Mixing in a thermohaline staircase. *Small-scale Turbulence and Mixing in the Ocean,* J. C. J. Nihoul and B. M. Jamart, Eds., Elsevier, 435–452.

——, 1994: Double diffusion in oceanography. *Ann. Rev. Fluid Mech.,* **26,** 255–285.

——, 1997: Macroscale signatures of double diffusion in the ocean. *Double-Diffusive Processes, 1996 Summer Study Program in Geophysical Fluid Dynamics,* S. Meacham and D. Tucholke, Eds., Woods Hole Oceanogr. Inst. Tech Rep. WHOI-97-10, 41–49.

——, H. Perkins, J. D. Boyd, and M. C. Stalcup, 1987: C-SALT: An investigation of the thermohaline staircase in the western tropical North Atlantic. *Deep-Sea Res.,* **34,** 1655–1665.

Shen, C. Y., 1989: The evolution of the double-diffusive instability: salt fingers. *Phys. Fluids A,* **1,** 829–844.

——, 1993: Heat-salt finger fluxes across a density interface. *Phys. Fluids,* **5,** 2633–2643.

——, 1995: Equilibrium salt-fingering convection. *Phys. Fluids,* **7,** 706–717.

Simpson, J. H., M. R. Howe, N. C. G. Morris, and J. Stratford, 1979: Velocity shear in the steps below the Mediterranean outflow. *Deep-Sea Res.,* **26A,** 1381–1386.

Stern, M. E., 1967: Lateral mixing of water masses. *Deep-Sea Res.,* **14,** 747–753.

——, 1969: Collective instability of salt fingers. *J. Fluid Mech.,* **35,** 209–218.

——, and J. S. Turner, 1969: Salt fingers and convecting layers. *Deep-Sea Res.,* **16,** 497–511.

Tait, R. I., and M. R. Howe, 1968: Some observations of thermohaline stratification in the deep ocean. *Deep-Sea Res.,* **15,** 275–280.

——, and ——, 1971: Thermohaline staircase. *Nature,* **231,** 178–179.

Taylor, J., and G. Veronis, 1986: Experiments on salt fingers in a Hele Shaw cell. *Science,* **231,** 39–41.

——, and P. Bucens, 1989: Laboratory experiments on the structure of salt fingers. *Deep-Sea Res.,* **36,** 1675–1704.

——, and G. Veronis, 1996: Experiments on double-diffusive sugar–salt fingers at high stability ratio. *J. Fluid Mech.,* **321,** 315–333.

Toole, J. M., and D. T. Georgi, 1981: On the dynamics of double-diffusively driven intrusions. *Progress in Oceanography,* Vol. 10, Pergamon, 123–145.

Turner, J. S., 1967: Salt fingers across a density interface. *Deep-Sea Res.,* **14,** 599–611.

——, 1968: The behavior of a stable salinity gradient heated from below. *J. Fluid Mech.,* **33,** 183–200.

Walsh, D., and B. Ruddick, 1995: Double-diffusive interleaving: The influence of nonconstant diffusivities. *J. Phys. Oceanogr.,* **25,** 348–358.

——, and ——, 1998: Nonlinear equilibration of thermohaline intrusions. *J. Phys. Oceanogr.,* **28,** 1043–1070.

——, and ——, 2000: Double-diffusive interleaving in the presence of turbulence—The effect of a nonconstant flux ratio. *J. Phys. Oceanogr.,* in press.

Whitfield, D. W. A., G. Holloway, and J. Y. Holyer, 1989: Spectral transform simulations of finite-amplitude double-diffusive instabilities in two dimensions. *J. Mar. Res.,* **47,** 241–265.

Williams, A. J., III, 1975: Images of ocean microstructure. *Deep-Sea Res.,* **22,** 811–829.

Zenk, W., 1970: On the temperature and salinity structure of the Mediterranean water in the northeast Atlantic. *Deep-Sea Res.,* **17,** 627–631.

Zhurbas, V. M., and R. V. Ozmidov, 1983: Formation of stepped fine structure in the ocean by thermohaline intrusions (English translation). *Izv. Atmos. Oceanic Phys.,* **19,** 977–982.

——, N. P. Kuzmina, and Ye. Kulsha, 1987: Step-like stratification of the ocean thermocline from transformations associated with thermohaline salt finger intrusions (numerical experiment) (English translation). *Oceanology,* **27,** 277–281.

——, J. J. Laanenets, R. V. Ozmidov, and V. T. Paka, 1988: Horizontal variability of thermohaline fields for stepped stratification in the ocean (English translation). *Oceanology,* **28,** 695–699.

Zodiatis, G., and G. P. Gasparini, 1996: Thermohaline staircase formations in the Tyrrhenian Sea. *Deep-Sea Res.,* **43,** 655–678.